Identifying mechanisms of initiation and maintenance of neuroendocrine prostate cancer

Alexandra N. Corella

A dissertation

submitted in partial fulfillment of the

requirements for the degree of

Doctor of Philosophy

University of Washington

2020

Reading Committee:

Peter S. Nelson, Chair

Colm Morrissey

David MacPherson

Program Authorized to Offer Degree:

Molecular and Cellular Biology

© Copyright 2020

Alexandra N. Corella

University of Washington

Abstract

Identifying mechanisms of initiation and maintenance of neuroendocrine prostate cancer

Alexandra N. Corella

Chair of the Supervisory Committee:

Peter S. Nelson

Professor, Department of Medicine, University of Washington

Small cell or neuroendocrine prostate cancer (SCNPC) is a rare but aggressive subtype of prostate cancer with no FDA-approved targeted therapies. SCNPC is an androgen-receptor independent subtype that often emerges as foci within conventional androgen-receptor dependent prostate cancers (ARPCs) that have undergone androgen-deprivation therapy (ADT). SCNPC and ARPC have highly similar mutational landscapes (including fusions in AR-regulated genes) but display distinct transcriptional programs. Investigations into the molecular mechanisms that are responsible for the development and maintenance of the neuroendocrine phenotype in prostate cancer have been hindered due to the scarcity of tumors and a lack of model systems with which to study the subtype.

Small cell or neuroendocrine tumors (SCNTs) arise in many organ sites throughout the body and have similar expression patterns of marker genes used to identify and diagnose this

class of tumors, including chromogranins and synaptophysins. In the following thesis, I conducted a transcriptome-wide comparison of SCNTs from different organ sites in order to identify related features. I found similar expression in thousands of genes among SCNTs, including transcription factors that may orchestrate the development of neuroendocrine gene expression programs and their downstream effectors, some of which may present as attractive therapeutic targets. I next evaluated the therapeutic efficacy of inhibiting two such targets using *in vitro* and *in vivo* models of SCNPC. Finally, I examined the role of the highly expressed SCNT-associated transcription factor, Insulinoma associated 1 (INSM1), in the development of the neuroendocrine phenotype in prostate cancer. Together this work provides novel insight into the molecular mechanisms that promote the initiation and maintenance of SCNPC.

TABLE OF CONTENTS

List of Figures

Acknowledgements

The following work could not have been completed without the help and support of my mentors, friends, and family.

To my mentor, Pete Nelson, thank you for giving me freedom to explore and discover my own research interests. To Pete and my committee members Colm Morrissey, David MacPherson, Toshi Tsukiyama, and Robert Bradley, thank you for your input and support over the years, through several iterations of this research and several scrapped projects. Your passion for science has shown through in our many discussions and will continue to be an inspiration to me as I continue my career in research.

To my lab members, especially Ruthy, Jared, Lauren, and Mick, thank you for suffering through my crazy ideas, helping me find my way, and being wonderful friends through my good and my bad times.

Thank you to the MCB program for your endless support and answering all of my questions big and small over the years.

To my MCB classmates, thank you for keeping me grounded in reality and for your comradery over the years. Thanks especially to Leisje and Becca for keeping joy in my life, and especially recently during the coronavirus quarantine.

Thank you to my family for supporting my seemingly never-ending academic career. Most especially, thank you to my husband, Marty, for letting me drag you to Seattle to pursue this degree. I could have never done it without your love and support and look forward to our next adventure.

Introduction

Globally, it is estimated that one man in eighteen will be diagnosed with prostate cancer in his lifetime [1]. In Western countries, the probability of diagnosis can be as high as one in eight (ACS facts and figures, 2019, https://www.cancer.org/content/dam/cancer-org/research/cancer-facts-and-statistics/annual-cancer-facts-and-figures/2019/cancer-facts-and-figures-2019.pdf). Prostate cancer is the most common type of cancer diagnosed in men and the leading cause of cancer death for men in over 50 countries [1]. Although the overall mortality rate of prostate cancer has been declining since the 1990s, this is largely due to the adoption of screening technologies leading to earlier detection of indolent disease [2]. The current five-year survival rate for men with localized disease upon diagnosis is 100%, whereas men who present with metastatic disease upon diagnosis have a five-year survival rate of 30.5% when compared to the general population (http://seer.cancer.gov/statfacts/html/prost.html.).

As the majority of all prostate cancer is initially driven by the androgen receptor (AR) signaling pathway, treatment strategies for men with metastatic disease typically consist of some form of androgen-deprivation therapy (ADT). ADT refers to the use of surgical or chemical methods to block androgen production or its activity. This therapeutic strategy is initially successful, but often leads to therapy resistance and the emergence of so-called “castration-resistant” prostate cancer (CRPC). A recent retrospective study of 127 men with prostate cancer found resistance to ADT developed in over 50% of patients within a period of less than two years [3]. Once castration-resistance is established, prognosis is poor. A separate study found that less than 50% of patients survived four years after the development of CRPC [4].

CRPC can be delineated into five major molecular subtypes based on the expression of genes indicating activity of the AR signaling pathway or the presence of a neuroendocrine gene

expression program [5]. The most prevalent CRPC subtype retains strong AR signaling activity without displaying neuroendocrine gene expression [6]. These AR-pathway driven prostate cancers (ARPCs) reactivate the AR-signaling program during ADT to promote growth and survival through a variety of mechanisms, including but not limited to, developing mutations or rearrangements in the AR and/or downstream genes, expanding ligand binding, or by manufacturing their own ligands [7-9].

Approximately 20% of CRPCs restore growth through signaling programs independent of AR [10, 11]. These AR-independent CRPCs predominantly fall into two categories: those with neuroendocrine gene expression and those without. Prostate cancer with neuroendocrine gene expression often displays "small cell" morphology consistent with other neuroendocrine carcinomas [12] and thus is commonly referred to as small-cell or neuroendocrine prostate cancer (SCNPC). Additional morphological subtypes of prostate cancer have been classified as neuroendocrine based on the presence of marker genes assessed by immunohistochemistry, however the clinical implications of these subtypes have been difficult to assess due to their rarity [13]. SCNPC is an aggressive variant of prostate cancer. Platinum-based chemotherapeutics have had some success in treating SCNPC [14], however there are no approved targeted therapies to date. In the ensuing study, I sought to identify and validate targeted therapeutic strategies for SCNPC.

Less than 2% of all prostate tumors exhibit SCNPC features upon diagnosis, however around 20% of autopsied men with CRPC have tumors with SCNPC features [15-17]. SCNPC has been observed to occur as foci within conventional ARPCs [12, 17, 18] and although these foci are AR-independent, they frequently contain the same mutations in AR (amplification in 67% of cases, [11]) and/or downstream target genes (TMPRSS2-ERG fusions, [19]) present in

the surrounding ARPC. The sum of these observations suggests that ARPC and SCNPC have either a common progenitor cell or that the SCNPC phenotype emerges under the selective pressure of ADT from the ARPC through a process of transdifferentiation. Treatment-induced transdifferentiation occurs in lung tumors, with Epidermal Growth Factor Receptor (EGFR) inhibition in adenocarcinomas leading to the development of small-cell lung cancer [20, 21]. The molecular mechanisms governing the initiation of SCNPC are poorly understood and are an active area of inquiry.

Although SCNPCs are often identified by the expression of a panel of neuroendocrine genes, a 2016 study by Beltran et. al [22] determined by whole-exome sequencing that the mutational landscapes of ARPC and SCNPC are largely similar. Instead, Beltran et al found that they could differentiate the two subtypes using a DNA methylation signature, implying that SCNPC and ARPC have distinct gene regulatory programs that manifest to drive the phenotype. In the following study, I examine the functional output of these gene regulatory programs in the form of transcriptomic data to identify and characterize molecular mechanisms promoting the initiation and maintenance of SCNPC.

Chapter 1. Small cell or neuroendocrine tumors from different organ sites have conserved transcriptional programs

*A version of the following work was published in:

Corella AN, , Cabiliza Ordonio MVA, Coleman I, Lucas JM, Kaipainen A, Nguyen HM, Sondheim D, Brown LG, True LD, Lee JK, MacPherson D, Nghiem P, Gulati R, Morrissey C, Corey E, Nelson PS. Identification of Therapeutic Vulnerabilities in Small-cell Neuroendocrine Prostate Cancer. Clin Cancer Res. 2019 Dec 5. doi: 10.1158/1078-0432.CCR-19-0775.

1.1 Abstract

Small-cell or neuroendocrine prostate carcinoma (SCNPC) is an aggressive subtype of prostate cancer with poor response to conventional therapies and no approved targeted therapies. The molecular mechanisms that drive the growth and survival of these tumors are poorly understood due to disease rarity and a lack of model systems for the subtype. SCNPC shares defining characteristics with other aggressive small-cell neuroendocrine tumors, such as “small-blue round cell” morphology and expression of chromogranin A. In this study, I compared whole transcriptome RNA-sequencing data from metastatic prostate cancer and two additional small cell or neuroendocrine tumor (SCNT) types, small cell lung cancer (SCLC) and Merkel Cell carcinoma (MCC). By differential expression analysis of each neuroendocrine tumor type to Androgen Receptor dependent prostate cancer (ARPC), I identified 4,988 genes exhibiting shared expression patterns in multiple neuroendocrine tumor types. Among these “pan-neuroendocrine” genes are known and novel transcription factors and lncRNAs associated with

SCNTs. Furthermore, I identified conserved expression patterns of druggable targets including those that have demonstrated efficacy in one or more SCNTs, such as BCL2.

1.2 Introduction

Like neuroendocrine neoplasms arising from different organ sites around the body, neuroendocrine prostate carcinomas can be categorized into separate pathological designations based on the morphology of the tumor cells [13]. In addition to shared morphologic features, neuroendocrine tumors from diverse organs can be identified by marker proteins frequently associated with neuronal or endocrine functions such as chromogranin A (CHGA), synaptophysin (SYP), and neural cell adhesion marker (NCAM) [23]. Neuroendocrine prostate tumors with aggressive clinical courses often display small-blue round cell morphology, so-called because they have a high nuclear to cytoplasmic ratio which causes the cells to appear almost wholly blue after staining with hematoxylin, a blue nuclear dye, and eosin, a pink cytoplasmic stain [24]. I refer to this collection of tumors as small cell or neuroendocrine prostate cancer (SCNPC).

In addition to shared physical and protein expression characteristics, a handful of shared mutations has been noted in aggressive small cell or neuroendocrine tumors (SCNTs). MYCN amplification and/or overexpression has long been associated with rapid progression of neuroblastoma and has more recently been described in subsets of small cell lung cancer (SCLC), as well as an estimated 40% of SCNPC cases [25-29]. Loss of the tumor suppressor gene RB1 is another common alteration in SCNTs, with loss estimated in 90% of SCNPC and loss of function mutations in over 90% of SCLC cases [27].

SCNPC, while increasing in frequency, is still a relatively rare form of castration-resistant prostate cancer (CRPC) [10]. Less than 1% of untreated prostate cancers present with small cell morphology [27]. The true prevalence of treatment-induced SCNPC has not been well characterized, however, a recent study identified small cell morphology in biopsies from 17% (27/160) of patients with CRPC [11]. The rarity of this tumor type translates into limited model systems with which to study the molecular features and dependencies of SCNPC in the laboratory. A growing number of patient-derived xenograft (PDX) models of SCNPC are becoming available, primarily through the University of Washington's Tissue Acquisition Necropsy (TAN) program [30]. However, for rapid molecular or therapeutic studies there exists only one widely accepted SCNPC cell line, NCI-H660. Upon its first derivation in 1985, the NCI-H660 cell line was initially classified as a "classic" SCLC cell line because the patient from which it was derived was diagnosed with SCLC based on histology, and the resulting cell line displayed four endocrine marker proteins commonly found in other SCLC cell lines [31]. NCI-H660 was later reclassified when it was found to have genomic characteristics of prostate tumors, including the TMPRSS2-ERG gene fusion [32].

Pan-cancer analyses have previously been used to identify molecular drivers and actionable drug targets in other tumor types. Similar morphological features, characteristic protein marker expression, gene mutations, and rapid disease progression suggest that SCNTs from different organ sites may have similar underlying transcriptional programs. To test this hypothesis, I compared RNA-sequencing data from SCNPC and two other SCNTs, Merkel cell carcinoma (MCC) and SCLC with Androgen Receptor-dependent prostate cancer (ARPC) samples to identify gene expression patterns associated with the SCNT phenotype.

1.3 Materials and Methods

Patient sample and RNA collection

Prostate cancer metastases were collected as part of the Prostate Cancer Donor Program at the University of Washington (UW). The collection of samples and RNA isolation of UW prostate cancer samples was carried out as previously described [10]. Merkel cell carcinoma patient samples and RNA were collected as part of a previously published study [33]. SCLC patient samples were obtained through the Cooperative Human Tissue Network. Collection of human samples was approved by the Institutional Review Board. SCLC cell lines NCI-H1436, NCI-H1672, NCI-H1963, NCI-H2141, NCI-H2195, NCI-H735, NCI-H774 were obtained from ATCC. RNA from tumor samples and cell lines was extracted with TRIzol (Invitrogen).

RNA-sequencing library prep and read processing

The purity and concentration of RNA was assessed by Nanodrop (Thermo Fisher) and Agilent Bioanalyzer. One microgram of total RNA was used as input to either the Illumina TruSeq RNA Library Kit v2 or the Illumina TruSeq Stranded mRNA Library prep kit and libraries were prepared and barcoded according to the manufacturer's protocol. Libraries were sequenced on the Illumina HiSeq 2500 generating either 50 or 75 base-pair paired end reads. Resulting reads were mapped to the hg38 human genome with TopHat v2.0.14 and transcript abundance was measured using the R Bioconductor package Genomic Alignments v1.18.0. Sequencing reads from patient-derived xenograft libraries were aligned to both hg38 human and mm10 mouse genomes. Reads that aligned with higher specificity to the mouse genome were removed as described [5] and remaining reads were processed as indicated for patient samples and cell lines.

Statistical Analyses

Differential expression analyses of RNA-sequencing data were carried out using the Bioconductor package edgeR v3.24.2 with transcript abundances as input. An FDR threshold of <0.05 was used as a cut-off for differential expression assessment. Multi-dimensional scaling analysis was conducted with all measured genes as input to the R Bioconductor package limma v3.38.3.

Calculation of AR and NE signature scores were carried out using the Bioconductor package GSVA v1.30.0 using z-score normalized log2 FPKM values as input. Scatterplots were created using ggplot2 v3.1.0 and the Pearson correlation between gene and signature score was calculated using the ggpubr v0.2 stat.cor() function.

Boxplots for individual genes were created with ggplot2 v3.1.0 and statistical assessment between groups was assessed by Student's t-test using the ggpubr v0.2 stat_compare_means() function.

Guilt-by-association analysis was performed by calculating the Pearson correlation between the log2FPKM expression of the lncRNA with that of each protein coding gene across all samples. Absolute values of the Pearson correlations were sorted, and the top 1% most highly correlated protein coding genes was used as input to identify enriched KEGG pathways with the gProfiler R package. Additional KEGG enrichment analysis was also performed with the gProfiler R package.

RNA-seq data from previously published datasets Bluemn et al., 2017, Aggarwal et al., 2018, and Abida et al. 2019 was analyzed and sample phenotypic groups were assigned for each cohort using classical multidimensional scaling (MDS) calculated with the cmdscale function in R on the expression profiles of 34 genes from the combined lists of "NEURO I", "NEURO II",

and “AR” gene signatures in Labrecque et al [5] and the “NE” and “AR” signatures in Bluemn et al. [10]. The distance metric was “euclidean” calculated by dist function on the columns (samples.)

1.4 Results

I combined whole transcriptome data comprising of eight MCC, 12 SCLC patient samples or cell lines, 116 CRPC metastases, including 25 from a previously published study [22]. All CRPC metastases were typed as SCNPC or ARPC based on a published 10-gene signature for activity of the Androgen Receptor (AR) signaling pathway and a 10-gene signature for neuroendocrine gene expression [10]. Ninety CRPC metastases were classified as ARPC due to a high AR-signature score (score $\geq +0.5$, on a scale from -1 to +1) and a low neuroendocrine signature score (score ≤ -0.5 on a scale from -1 to +1) and 26 were classified as SCNPC for displaying the inverse phenotype (Figure 1.1A). The other SCNTs profiled in this study also display high expression of the 10-gene signature for neuroendocrine gene expression, with the exception of NKX2-1 in MCC (Figure 1.1A). The absence of expression of NKX2-1 (or TTF1) has previously been noted to distinguish MCC from other SCNTs [34, 35]. Multi-dimensional scaling analysis based on the expression of all genes captured by RNA-sequencing divided samples into two groups, one consisting of ARPC samples and the other containing SCNPC, MCC, and SCLC samples (Figure 1.1B).

Differential expression analysis between ARPC and SCNPC samples revealed over half of all genes, 12,318 out of 20,413 genes measured, were differentially expressed using the FDR threshold of 0.05. The 817 most highly differentially expressed genes between ARPC and

SCNPC ($|\log_2$ fold change$|$ >4) displayed similar patterns of expression across all three SCNTs assessed (Figure 1C).

To identify genes with consistent expression patterns across SCNTs, each SCNT type was compared to ARPC. 4,988 genes with differential expression (FDR<0.05) between each SCNT and ARPC and the same direction of change across all three SCNTs were categorized as pan-neuroendocrine genes. The pan-neuroendocrine genes that are upregulated when compared to ARPC are enriched for KEGG pathways associated with neuronal and cell cycle processes (Figure 1.1D). In the following sections, I separate these pan-neuroendocrine genes into functional classes to highlight their potential roles in the SCNT phenotype.

1.4.1 Pan-neuroendocrine transcription factors

I compiled a list of human transcription factors based on annotations in the Functional Annotation of the Mammalian Genome Consortium (FANTOM) database and genes that associated with the Gene Ontology term "TF activity" in the AmiGO database. Of the 4,988 pan-neuroendocrine genes, 444 met this criterion for a transcription factor. Many of these transcription factors are known to be involved in the development of neuronal or neuroendocrine cells and are highly expressed in other SCNTs, including SOX2, NEUROD1, and HES6 (Figure 1.2A). The top differentially regulated transcription factor between ARPC and the SCNTs is ST18, a factor with previously described roles in neuronal development and pancreatic endocrine cells [36, 37].

MYT1L, another highly expressed pan-neuroendocrine transcription factor, maintains neuronal phenotypes in cells by repressing pathways that instruct non-neuronal fates, such as Notch signaling [38]. In addition, expression of MYT1L along with BRN2 and ASCL1 was

recently demonstrated to be sufficient to reprogram fibroblasts into neurons [39]. MYT1L expression was also found to be positively correlated with worse prognosis in another SCNT, medulloblastoma [40].

Amplifications in the MYC gene family have been noted in many cancers. In prostate, MYC amplification or upregulation in ARPC is associated with poor prognosis [41-43]. MYCN amplification or overexpression has been associated with SCNPC [29]. Consistent with previous findings, MYC is most highly expressed in ARPC compared to the SCNT tumor panel (Figure 1.2B). Overall, MYCN is elevated among the SCNTs, but displays a wide range of expression in SCLC samples (Figure 1.2C). Of note, MYCL, recently implicated in the initiation of SCLC [44], is also highly expressed across the SCNTs sampled (Figure 1.2D).

1.4.2 Pan-neuroendocrine long non-coding RNAs

Long non-coding RNAs have been proposed to have highly tissue specific and cancer specific functions [45-47]. In prostate cancer, many lncRNAs, including HOTAIR and Schlap-1 have been found to positively correlate with proliferation and invasion of tumor cells [48, 49]. To identify SCNT-associated lncRNAs, I first compiled a list of known transcripts classified as a type of lncRNA or "pseudogene" from ENSEMBL and NCBI GRch38 annotations. Of 2,283 total lncRNAs captured by RNA-seq, 447 are consistently expressed across SCNTs (Figure 1.3A). As most lncRNAs have no ascribed functions, I used guilt-by-association analysis of the top 50 most highly expressed pan-neuroendocrine lncRNAs with protein-coding genes in order to determine which molecular pathways these lncRNAs may contribute. Among the most highly enriched KEGG pathways are those related to neuronal processes and DNA repair pathways (Figure 1.3B). Prostate cancer was also determined to be a highly enriched pathway associated

with pan-neuroendocrine lncRNAs. I cross-referenced the pan-neuroendocrine lncRNAs with a recent study characterizing lncRNA expression in SCNPC and found that many of the pan-neuroendocrine lncRNAs increase with the development of resistance to ADT [50]. Overall, there was a high concordance of lncRNA expression across SCNTs. Of 122 lncRNAs upregulated in SCNPC compared to ARPC, 100 (80%, $p<0.0001$) of these were also upregulated in MCC and SCLC compared to ARPC.

1.4.3 Profiling "druggable" targets in SCNTs

In addition to characterizing general expression features of SCNTs, a major motivation for this study was to identify candidate therapeutic targets for further evaluation. To this end, I used a previously published list of genes comprising the "druggable" genome to assess which targets were enriched in SCNTs [51]. Out of 4,026 druggable genes captured by RNA-seq, 875 are associated with SCNTs (Figure 1.4A). These druggable targets include many cell surface proteins that are currently or have previously been studied for exploitation by immunotherapy or targeted antibody or small molecule-based therapies. DLL3, a Notch ligand receptor, is highly upregulated in SCNTs over ARPC (Figure 1.4B). Rovalpituzumab-teserine, an antibody-drug conjugate directed at DLL3, has demonstrated clinical efficacy in SCLC in on-going trials [52].

Additional highly expressed druggable targets in SCNTs include those currently being investigated, among them, AURKA, AURKB, and the BET family member BRD4. BET inhibitors have been found to induce apoptosis in pre-clinical models of SCLC [53]. BET inhibitors have also been found to have efficacy in tumors with elevated MYC family member expression, with sensitivity associating with MYCN in neuroblastoma and MYCL in SCLC [54, 55]. BET inhibitors are currently being studied in a variety of prostate cancer subtypes [56].

Notably, BCL2 is among the most highly upregulated druggable targets across SCNTs (Figure 1.4C). Pharmacologic inhibition and genetic knockdown induce apoptosis in both SCLC and MCC, but have not been assessed in SCNPC [57, 58]. I examined three additional published datasets for BCL2 expression in prostate cancer and found similar upregulation in SCNPC over ARPC samples (Figure 1.4D-F). Future chapters detail studies of BCL2 inhibition in SCNPC.

1.5 Discussion

Historically, tumors have been classified and analyzed according to their organ of origin. More recently, pan-cancer efforts such as those being conducted by The Cancer Gene Atlas Network (TCGA) have sought to assess similarities in oncogenic signaling across tumors with different cells of origin [59, 60]. The TCGA studies thus far have been focused on primary tumors from more common malignancies. Although neuroendocrine neoplasms are increasing in frequency [61], there remain subtypes of SCNTs, like SCNPC, that are still relatively rare and have limited model systems to study. With this study, I highlight shared transcriptome features, including transcription factors that activate neuronal or neuroendocrine gene expression programs, lncRNAs that promote growth and invasion, and a number of druggable targets across three SCNTs in order to identify candidate genes for future research into the mechanisms of initiation and maintenance of SCNTs.

MYCN has been implicated in many SCNTs, including neuroblastoma, SCNPC, and SCLC, in promoting cellular plasticity [62, 63]. I identified that another MYC family member, MYCL, previously found to foster SCLC initiation [44] is highly expressed in both MCC and SCNPC. In total, 444 transcription factors were determined to have pan-neuroendocrine

expression profiles. Further work is necessary to determine whether these factors contribute to the development or support the phenotype of SCNTs.

LncRNAs, once thought to be "junk" transcripts, are increasingly recognized for having functional roles in many diseases, including cancer. Due to their tendency to be expressed in a tissue-specific manner, lncRNAs are also increasingly included in biomarker panels for diagnosis and staging of disease [64]. I identified 447 lncRNAs with conserved expression patterns across the SCNTs profiled. The most highly expressed of these lncRNAs are positively correlated with protein-coding genes involved in KEGG pathways related to prostate cancer. Among the most highly expressed lncRNAs, MIAT has been previously associated with SCNPC [65], however other lncRNAs like LINC01346 currently have no ascribed functions in prostate cancer or SCNTs.

The aggressive clinical course of SCNTs and a lack of targeted therapies drove me to focus on identifying potential therapeutic approaches. In addition to bromodomain inhibitors, Aurora Kinase inhibitors are being investigated clinically and have had some efficacy in the context of MYCN-amplified SCNPC [66]. BCL2 has been known to be highly expressed in SCNPC and other SCNTs for decades [67, 68]. With recent studies demonstrating promising pre-clinical results of BCL2 inhibitors in SCLC and MCC [57, 58], I next chose to evaluate BCL2 as a therapeutic target in SCNPC.

1.6 Figures

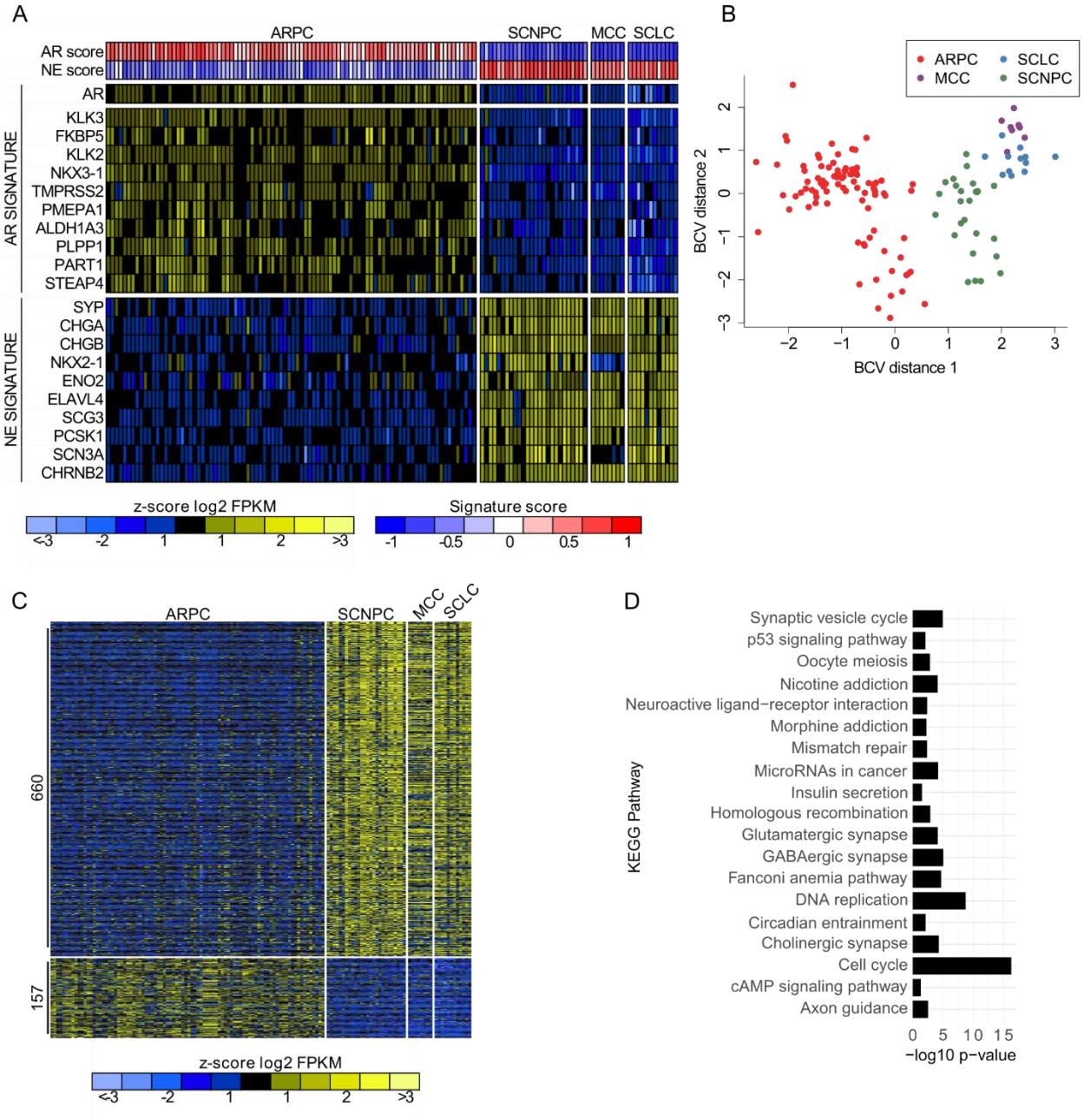
A
ARPC
SCNPC
MCC
SCLC
AR score
NE score
AR
AR SIGNATURE
KLK3
FKBP5
KLK2
NKX3-1
TMPRSS2
PMEPA1
ALDH1A3
PLPP1
PART1
STEAP4
NE SIGNATURE
SYP
CHGA
CHGB
NKX2-1
ENO2
ELAVL4
SCG3
PCSK1
SCN3A
CHRNB2
z-score log2 FPKM
<-3 -2 1 1 2 >3
Signature score
-1 -0.5 0 0.5 1
B
ARPC
SCLC
MCC
SCNPC
BCV distance 2
BCV distance 1
C
ARPC
SCNPC
MCC
SCLC
660
157
z-score log2 FPKM
<-3 -2 1 1 2 >3
D
KEGG Pathway
Synaptic vesicle cycle
p53 signaling pathway
Oocyte meiosis
Nicotine addiction
Neuroactive ligand−receptor interaction
Morphine addiction
Mismatch repair
MicroRNAs in cancer
Insulin secretion
Homologous recombination
Glutamatergic synapse
GABAergic synapse
Fanconi anemia pathway
DNA replication
Circadian entrainment
Cholinergic synapse
Cell cycle
cAMP signaling pathway
Axon guidance
0 5 10 15
−log10 p−value

Figure 1.1 Neuroendocrine carcinomas originating in different organ sites share gene expression programs. (**A**) Heatmap showing relative transcript levels measured by RNA sequencing of AR-signature genes and neuroendocrine signature genes across patient metastases and cancer cell lines. (**B**) Multidimensional scaling analysis of samples across all genes measured by RNA-sequencing. (**C**) Heatmap of top 817 differentially expressed genes (|log2 fold change| >4, FDR 0.05) in SCNPC versus ARPC tumors with expression shown across all samples. (**D**) KEGG pathways enriched in top upregulated pan-neuroendocrine genes.

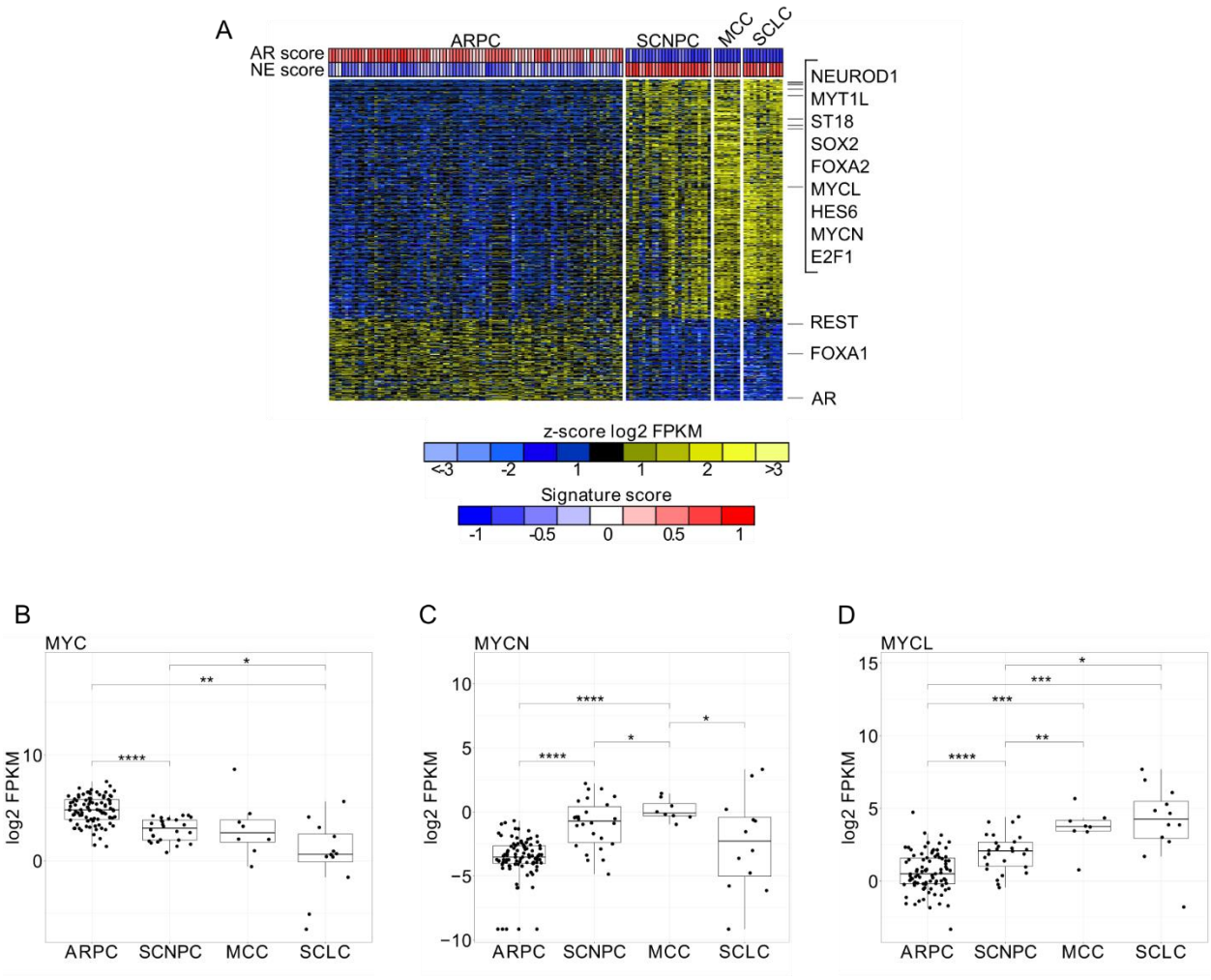

Figure 1.2 SCNTs express transcription factors associated with neuroendocrine gene expression. (**A**) Heatmap of the expression 444 transcription factors differentially expressed between ARPCs and neuroendocrine cancers. (**B-D**) Expression levels of MYC family members across tumor subtypes determined by RNA-seq (*, $p<0.05$; **, $p<0.01$; ***, $p<0.001$; ****, $p<0.0001$ by Student t test).

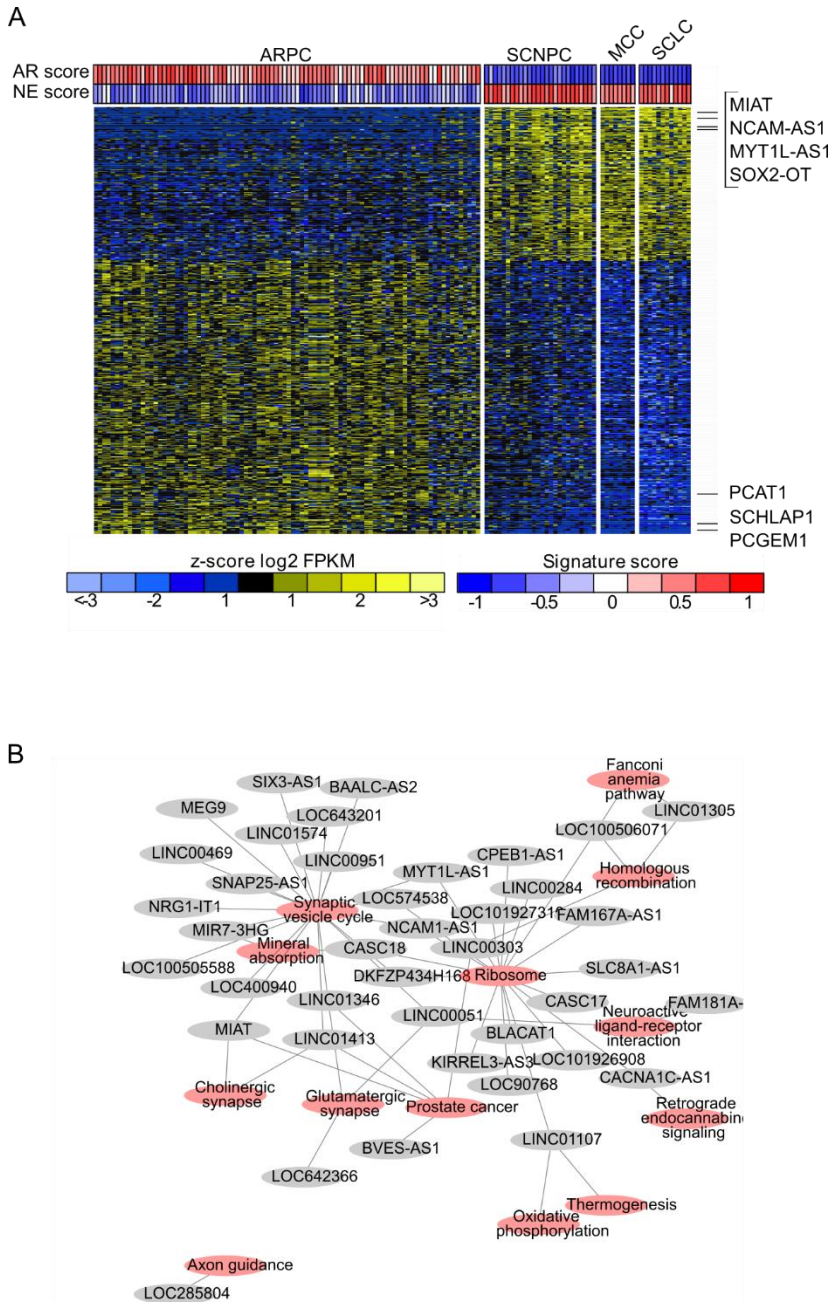

Figure 1.3 LncRNAs associated with SCNTs. (**A**) Heatmap displaying expression of pan-neuroendocrine lncRNAs. (**B**) Guilt by association analysis displaying KEGG pathways enriched in most highly correlated protein coding genes with the top 50 most upregulated pan-neuroendocrine lncRNAs.

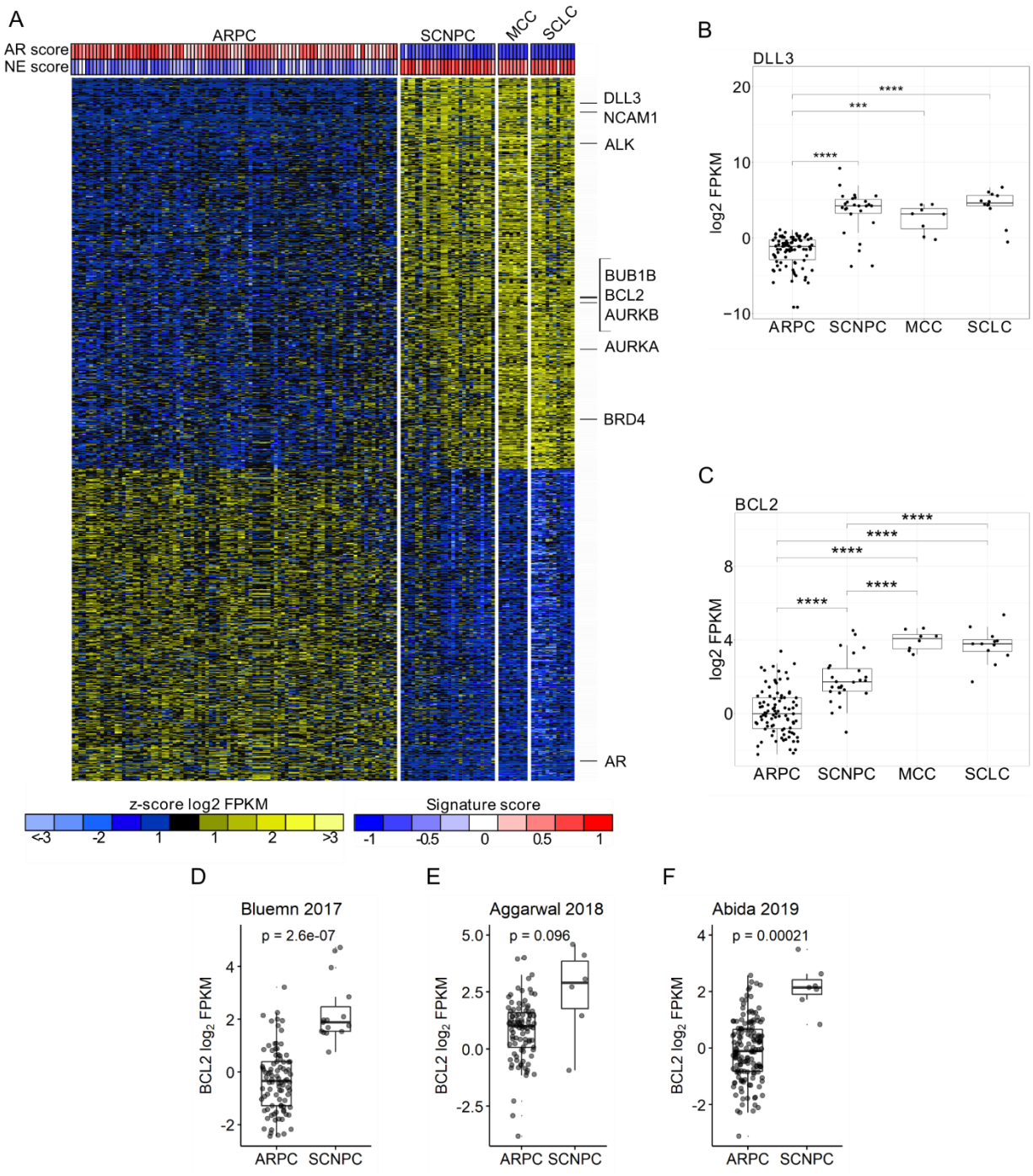
A
ARPC
SCNPC
MCC
SCLC
AR score
NE score
DLL3
NCAM1
ALK
BUB1B
BCL2
AURKB
AURKA
BRD4
AR
z-score log2 FPKM
<-3
-2
1
1
2
>3
Signature score
-1
-0.5
0
0.5
1
B
DLL3
log2 FPKM
20
10
0
−10
****
***
****
ARPC
SCNPC
MCC
SCLC
C
BCL2
log2 FPKM
8
4
0
****
****
****
****
****
ARPC
SCNPC
MCC
SCLC
D
Bluemn 2017
p = 2.6e-07
BCL2 log2 FPKM
4
2
0
-2
ARPC
SCNPC
E
Aggarwal 2018
p = 0.096
BCL2 log2 FPKM
5.0
2.5
0.0
-2.5
ARPC
SCNPC
F
Abida 2019
p = 0.00021
BCL2 log2 FPKM
4
2
0
-2
ARPC
SCNPC

Figure 1.4 Profiling the druggable genome across SCNTs. (**A**) Heatmap displaying genes in the druggable genome with differential expression between ARPCs and neuroendocrine tumors. (**B**) Expression of the transcript encoding the cell surface notch pathway gene DLL3. (**C**) Expression of transcripts encoding BCL2 across tumor subtypes. (**D–F**) Boxplots depicting BCL2 transcript levels measured by RNA-sequencing in metastatic tumors from patients with CRPC. (***, $p<0.001$; ****, $p<0.0001$ by Student t test).

Chapter 2. Small cell or neuroendocrine prostate cancer is sensitive to dual BCL2 and WEE1 inhibition

*A version of the following work was published in:

Corella AN, Cabiliza Ordonio MVA, Coleman I, Lucas JM, Kaipainen A, Nguyen HM, Sondheim D, Brown LG, True LD, Lee JK, MacPherson D, Nghiem P, Gulati R, Morrissey C, Corey E, Nelson PS. Identification of Therapeutic Vulnerabilities in Small-cell Neuroendocrine Prostate Cancer. Clin Cancer Res. 2019 Dec 5. doi: 10.1158/1078-0432.CCR-19-0775.

2.1 Abstract

Small cell or neuroendocrine prostate cancer (SCNPC) is a subtype with poor clinical outcomes and for which there are no FDA-approved targeted therapeutics. To identify candidate therapies for pre-clinical evaluation, I conducted a transcriptome analysis of the druggable genome in patient metastases. From this analysis, I identified BCL2 as elevated in SCNPC. BCL2 inhibition leads to apoptotic cell death of SCNPC cell lines and reduces the growth of some SCNPC patient-derived xenograft models. I also determined that the mitotic kinase WEE1 is overexpressed in SCNPCs. Combining the BCL2 inhibitor ABT-263 with the WEE1 inhibitor AZD-1775 results in a synergistic decrease of viability and growth in several SCNPC pre-clinical models. The combination of BCL2 and WEE1 inhibition may present a novel therapeutic strategy for the treatment of SCNPC.

2.2 Introduction

Although potent targeted therapies exist for androgen receptor-driven prostate cancers (ARPCs), there are currently no FDA approved targeted therapies for the treatment of small-cell or neuroendocrine prostate cancer (SCNPC). SCNPC is commonly treated with platinum-based chemotherapies due to its similar genetic and morphological characteristics with small-cell lung cancer (SCLC) where platinum and etoposide are used as standard first-line therapy and have some success [14, 69]. While markers predicting response to platinum-based chemotherapies in SCNPC have been identified, the underlying biology governing this response is not currently understood [14].

There are several targeted therapies undergoing evaluation for efficacy in aggressive prostate cancers, including SCNPC. Among these are agents indirectly targeting the previously described SCNPC oncogenic driver MYCN [29, 70], including Bromodomain and Extra-Terminal motif (BET) inhibitors and Aurora kinase inhibitors. Amplification or overexpression of MYCN has long been associated with other neuroendocrine tumor types, including neuroblastoma and SCLC [27, 28, 71, 72]. Single-agent BET inhibitor trials thus far have focused broadly on castration-resistant prostate cancer (CRPC) and early phase studies have shown modest activity with several patients achieving a partial response [73]. BET inhibitors are now being administered in combination with androgen-deprivation therapies in ongoing trials (NCT02711956, NCT02607228). The Aurora kinase inhibitor, Alisertib, has been evaluated for efficacy in patients exhibiting clinical characteristics of SCNPC with very limited overall response rates. However exceptional responses were observed in a small number of patients with elevated MYCN and AURKA [66].

A lack of targeted therapies represents a critical unmet need for patients with SCNPC. The rarity of the SCNPC subtype and a lack of model systems have contributed to the dearth of knowledge surrounding the molecular mechanisms that drive the growth of SCNPC and resistance to chemotherapy. As described in chapter 1, I profiled the "druggable genome" across a panel of small cell or neuroendocrine tumors (SCNTs) to identify candidate targets for evaluation in SCNPC. In this study, I present data on the pre-clinical efficacy of dual BCL2 and WEE1 inhibition in SCNPC.

2.3 Materials and Methods

Patient sample and RNA collection

Prostate cancer metastases were collected as part of the Prostate Cancer Donor Program at the University of Washington. The collection of samples and RNA isolation of UW prostate cancer samples was carried out as previously described [10]. Merkel cell carcinoma patient samples and RNA were collected as part of a previously published study [33]. SCLC patient samples were obtained through the Cooperative Human Tissue Network. Collection of human samples was done with the approval of the Institutional Review Board. SCLC cell lines NCI-H1436, NCI-H1672, NCI-H1963, NCI-H2141, NCI-H2195, NCI-H735, NCI-H774 were obtained from ATCC. RNA from tumor samples and cell lines was extracted with TRIzol (Invitrogen).

RNA-sequencing library prep and read processing

The purity and concentration of RNA was assessed by Nanodrop (Thermo Fisher) and Agilent Bioanalyzer. One microgram of total RNA was used as input to either the Illumina Tru

Seq RNA Library Kit v2 or the Illumina TruSeq Stranded mRNA Library prep kit and libraries were prepared and barcoded according to the manufacturer's protocol. Libraries were sequenced on the Illumina HiSeq 2500 generating either 50 or 75 base-pair paired end reads. Resulting reads were mapped to the hg38 human genome with TopHat v2.0.14 and transcript abundance was measured using the R Bioconductor package Genomic Alignments v1.18.0. Sequencing reads from patient-derived xenograft libraries were aligned to both hg38 human and mm10 mouse genomes. Reads that aligned with higher specificity to the mouse genome were removed as described [5] and remaining reads were processed as indicated for patient samples and cell lines.

Statistical Analyses

Differential expression analyses of RNA-sequencing data were carried out using the Bioconductor package edgeR v3.24.2 with transcript abundances as input. An FDR threshold of <0.05 was used as a cut-off for differential expression assessment. Multi-dimensional scaling analysis was conducted with all measured genes as input to the R Bioconductor package limma v3.38.3.

Calculation of AR and NE signature scores were carried out using the Bioconductor package GSVA v1.30.0 using z-score normalized log2 FPKM values as input. Scatterplots were created using ggplot2 v3.1.0 and the Pearson correlation between gene and signature score was calculated using the ggpubr v0.2 stat.cor() function.

Boxplots for individual genes were created with ggplot2 v3.1.0 and statistical assessment between groups was assessed by Student's t-test using the ggpubr v0.2 stat_compare_means() function.

Guilt-by-association analysis was performed by calculating the Pearson correlation between the log2FPKM expression of the lncRNA with that of each protein coding gene across all samples. Absolute values of the Pearson correlations were sorted, and the top 1% most highly correlated protein coding genes was used as input to identify enriched KEGG pathways with the gProfiler R package. Additional KEGG enrichment analysis was also performed with the gProfiler R package.

RNA-seq data from previously published datasets Bluemn et al., 2017, Aggarwal et al., 2018, and Abida et al. 2019 was analyzed and sample phenotypic groups were assigned for each cohort using classical multidimensional scaling (MDS) calculated with the cmdscale function in R on the expression profiles of 34 genes from the combined lists of "NEURO I", "NEURO II", and "AR" gene signatures in Labrecque et al [5] and the "NE" and "AR" signatures in Bluemn et al. [10]. The distance metric was "euclidean" calculated by dist function on the columns (samples).

Cell Lines

The cell lines, LNCaP (ATCC), C4-2 (ATCC), MSKCC EF1 (gift from John K. Lee), MKL-1 (Sigma), VCaP (ATCC), LAPC4 (gift of Charles Sawyers), NCI-H660 (ATCC), NCI-H82 and NCI-H69 (ATCC), MS-1 (Sigma) were maintained in a 37ºC incubator with 5% CO_2 and grown in medium supplemented with fetal bovine serum and other additives as recommended by ATCC or the cell line provider. STR genotyping was used to authenticate the lines and cells were confirmed to be myco-plasma free using the MycoAlert Detection Kit (Lonza, LT07-418). Cells were cultured no longer than 10 passages after thawing and before experimental use.

Protein isolation and immunoblotting

Cell lines were washed 1x with PBS prior to the addition of a cell lysis buffer (1.5 M Urea, 1% SDS, 1% NP-40, 2% Tween20, 250 nM NaCl, PBS) supplemented with 1x phosphatase inhibitors (PhosStop, Roche Diagnostics) and a 1x protease inhibitor cocktail (Complete Mini, Roche Diagnostics). PDX tissues were pulverized in liquid nitrogen with a mortar and pestle prior to the addition of lysis buffer. Lysates were sonicated and then centrifuged to clear debris. Protein quantification was performed using the Pierce bicinchoninic acid assay (Thermo Scientific). Lysates were mixed with LDS sample buffer and Reducing Agent (NuPage) and heated at 70ºC for 10 minutes. Lysates were run on a 4-12% NuPage Bis-Tris gel and protein was transferred to a nitrocellulose membrane in Tris/CAPS buffer using a semi-dry transfer apparatus. Membranes were blocked and incubated with antibody solutions in 5% milk powder in 1x PBS with 0.01% Tween. Primary anti-bodies targeting BCL2 (Santa Cruz Biotechnologies, sc-7382, 1:500), BCL-XL (Cell Signaling, 2764, 1:1000), BCLW (Cell Signaling, 2724, 1:1000), Cleaved Caspase-3 (Cell Signaling, 9661S, 1:1000), WEE1 (Cell Signaling, 13084, 1:1000) phospho-cdc2(Tyr15) (Cell Signaling, 4539, 1:1000), AR (Abcam, ab133273, 1:2000), PSA (Santa Cruz Biotechnologies, sc7638, 1:100) and GAPDH (BioRad, hFAB Rhodamine, cat# 12004167, 1:5000) were used. Secondary antibodies used were Goat-anti-Rabbit (Goat anti-Rabbit IgG (H+L) Secondary Antibody, HRP cat# 31460, 1:5000) and Goat-anti-Mouse (BioRad, StarBright Blue 700 cat# 12004158, 1:5000). Blots were imaged using the ChemiDoc MP (BioRad).

Immunohistochemistry

LuCaP tissue microarrays (TMAs) were constructed and stained as previously described [74]. Antibodies directed toward the detection of BCL2 [EPR17509] (Abcam, cat# ab182858) p-CDK1 (Abcam, ab-133463) and Wee1 (Santa Cruz Biotechnologies, sc-5258) were used according to the manufacturer's instructions. Staining assessment was blinded, and the H-score was calculated and averaged across multiple tissue/tumor cores for the same LuCaP PDX line.

Drug treatments of cell lines.

Cell lines were seeded in 96-well plates in 50 µl media 24 hours before the addition of the inhibitor. Serial dilutions of inhibitors were made in media and 50 µl of a 2x inhibitor solution were added to plates containing cells. At least three technical replicates for each dose were plated. The maximal amount of DMSO for each serial dilution was used as a vehicle control for all dose points. Viability was assessed 96 hours after addition of inhibitor using the Cell Titer-Glo 2.0 Assay (Promega), following the manufacturer's protocol. Dose-response curves shown are an average and standard deviation of 3 biological replicates for each cell line and each inhibitor. Non-linear regression curves were fitted to the average of biological replicates in GraphPad Prism7. Inhibitors used were ABT-199 (Selleckchem, S8048), ABT-263 (Selleckchem, S1001), Gambogic Acid (Selleck-chem, S2448), A-1155463 (Selleckchem, S7800), and AZD-1775 (Selleckchem, S1525).

For assessment of cell death with cleaved caspase-3 immunoblot, cells were plated in 10 cm dishes in media. After 24 hours, the media was changed to media containing DMSO or 100 nM ABT-263. Cells were harvested 24 hours post-addition of drug and lysates collected as described.

Tumor Dissociation and Drug Treatment

LuCaP patient derived xenograft (PDX) tumors were obtained from the University of Washington. After resection and mincing, tumor pieces were placed in digestion media containing 1 mg/mL collagenase and 1 mg/mL dispase. The tumor mixture was incubated at 37°C for 1 hour. Digested tissue was passed through 20 G needle six times. The mixture was passed through 100 m and 40 m filters before counting. Cells were plated in 6-well dishes and treated with either vehicle (DMSO), AZD-1775 (500 nM final concentration), ABT-263 (final 10 nM) or the combination AZD-1775 and ABT-263 (500 nM + 10 nM). After 72 hours, protein was harvested.

siRNA treatment of cell lines

Cells were plated 24 hours before transfection in 6-well or 96-well plates. Cells were transfected with 60 nM (final concentration) Non-targeting siRNA (Dharmacon, cat # D-001206-13-20, siGENOME Non-Targeting siRNA Pool #1) or BCL2 siRNA (Dharmacon, cat# M-003307-06-0010, SMARTpool: SiGENOME BCL2 siRNA) using TransIT-TKO Transfection Reagent (Mirus, cat# MIR 2154) following the manufacturer's instructions. Protein was collected and viability was assessed 96 hours post transfection. Data shown are an average and standard deviation of three biological replicates.

Patient derived xenograft studies

All animal procedures were approved by UW Institutional Animal Care and Use Committee (IACUC) and according to NIH guidelines. Male mice (n=24 per PDX model) were implanted subcutaneously with tumor bits using a trocar. We used LuCaP 49, LuCaP 93, LuCaP

173.1, LuCaP 145.1, and LuCaP 145.2 SCNPC PDX models. When tumors reached ~100 mg, animals were randomized to treatment groups. We were aiming for three animals with tumor per arm: 1) control, 2) ABT-263; 3) AZD-1775, 4) ABT-263+AZD-1775. ABT-263 was formulated at 50 mg/kg in 10% ethanol, 30% polyethylene glycol 400 and 60% Phosal 50PG and AZD1775 was formulated at 60 mg/kg in 0.5% w/v methyl cellulose. Both drugs were administered by oral gavage once a day, with five days on-two days off regimen. In the combination group ABT-263 was administered first and AZD-1775 90 minutes later. Treatments were administered for four weeks. Tumor volume and body weight were measured twice a week. Animals were sacrificed at four weeks, when tumors exceed 1000 mg or when animal health was compromised.

2.4 Results

2.4.1 BCL2 is upregulated in SCNPC patient samples

Using whole-transcriptome RNA-sequencing data generated from patient metastases and cell lines, I identified BCL2 as highly upregulated in SCNPC and in two other SCNTs, Merkel Cell carcinoma (MCC) and small cell lung cancer (SCLC) (Figure 2.1A). Consistent with this expression pattern, BCL2 RNA levels are positively correlated with a 10-gene neuroendocrine (NE) signature score and negatively correlated with a 10-gene androgen receptor (AR) activity score (Figure 2.1B, 2.1C, [10]). Although modern BCL2 inhibitors have high inhibitory selectivity for BCL2, they can bind other anti-apoptotic BCL2 family members, including BCLXL and BCLW. BCLW is downregulated in all SCNTs profiled compared to ARPC samples (Figure 2.1D) and has a negative correlation with the NE signature score and positive correlation to the AR-activity score (Figure 2.1E, F). BCLXL displays similar expression across all tumor types and has no correlation to AR or NE gene signatures (Figure 2.1G-I).

2.4.2 BCL2 is upregulated in *in vitro* and *in vivo* models of SCNPC

Prior to conducting *in vitro* and *in vivo* testing of BCL2 inhibitors in SCNPC models, I first assessed whether the expression of BCL2 and its commonly co-targeted family members mirrored the patient data. Using a panel of cell lines representing the tumor types in our transcriptome dataset, I determined by Western Blot that BCL2 protein is highly expressed across most SCNT cell lines (Figure 2.2A), while it is low or undetectable in the ARPC lines assayed. The outlier among the SCNT cell lines profiled is NCI-H82, which displays low BCL2 and high BCLW protein by Western Blot. Low BCL2 expression and resistance to the BCL2 inhibitor, ABT-199, has been observed in NCI-H82 [57]. Both BCLXL and BCLW protein are present in all cell lines assessed but neither protein demonstrated a clear correlation with tumor type.

Using whole-transcriptome RNA-sequencing data from the University of Washington's LuCaP series of prostate cancer patient-derived xenograft (PDX) models, I determined that BCL2 is highly upregulated in SCNPC PDX models compared to ARPC models (Figure 2.2B). BCL2 expression is also positively correlated with the NE signature score in PDX models (Figure 2.2C). BCL2 protein is also elevated in SCNPC PDX models as assessed by Western Blot and immunohistochemistry (IHC) (Figure 2.2D, E, respectively). Consistent with cell line findings, BCLXL and BCLW protein are detectable in all PDX samples regardless of phenotype (Figure 2.2D).

2.4.3 BCL2 inhibition leads to apoptotic cell death in SCNPC cell lines

Treatment of a panel of ARPC (LNCaP, C4-2, LAPC4, VCaP) and SCNPC (NCI-H660, MSKCC EF1) cell lines with two inhibitors more selective to BCL2, ABT-263 and ABT-199,

revealed that SCNPC lines were more sensitive to BCL2 inhibition than ARPC lines (Figure 2.3A,B). To assess whether off-target inhibition of other BCL2 family members contributed to the drastic reduction of viability in SCNPC lines, I carried out dose-response experiments with inhibitors more selective to other BCL2 family members, akin to a published pharmacologic approach to "BH3 profiling" [75]. No differential sensitivity to inhibitors that more selectively target BCLXL or BCLW (A1155463 and Gambogic Acid, respectively) was observed in the panel of cell lines (Figure 2.3C, D). Older generation BCL2 family inhibitors including ABT-737, Sabutoclax, Obatoclax, and a MCL-1 selective inhibitor, A1210477 were also tested (Figure 2.3E-H). Of these inhibitors, the SCNPC line NCI-H660 was differentially sensitive to the tool compound, ABT-737, which targets BCL2 and BCLXL with high affinity (Figure 2.3E). A 24-hour treatment with 100 nM ABT-263 induced caspase-3 cleavage in NCI-H660 but not the ARPC lines, C4-2 and LNCaP, as assessed by Western Blot (Figure 2.3I).

Although only modest knockdown of BCL2 was achievable by siRNA in the NCI-H660 cell line, a significant decrease in viability was observed 96 hours post transfection compared to the ARPC cell line, LNCaP (Figure 2.3J-M).

2.4.4 BCL2 inhibition reduces growth of some SCNPC PDX models

In collaboration with Dr. Eva Corey at the University of Washington, a panel of SCNPC PDX models was treated with the BCL2 inhibitor, ABT-263. Of the five models tested, two displayed a significant reduction in growth over a four-week period (Figure 2.4A). The responding models, LuCaP 49 and LuCaP 173.1, had end of study tumor volumes approximately four times less than those of vehicle treated tumors. To begin to assess whether resistance in non-responding models could be attributed to another BCL2 family member, I profiled

additional pro- and anti-apoptotic BCL2 family proteins in the PDX models (Figure 2.4B). The pro-apoptotic proteins BAX and BAK appear to be lower in LuCaP 49 and LuCaP 173.1 compared to models that were resistant to ABT-263. This data suggests that sensitive models are more reliant on the previously described ability of BCL2 to directly or indirectly neutralize the activity of BAX and/or BAK [76], however complete profiling of BCL2 family proteins is necessary to confirm this hypothesis. In the absence of cell line models that emulate the heterogeneity of response to ABT-263 observed in the SCNPC PDX models, I chose to focus on finding additional candidate therapeutic targets to evaluate in SCNPC.

2.4.5 WEE1 is upregulated in SCNPC

Returning to my analysis of the "druggable genome" in SCNTs, I determined that WEE1 is differentially upregulated in MCC and SCLC compared to ARPC ($p<0.05$), and trended toward elevated expression in SCNPC apart from a few outliers (Figure 2.5A). I determined that WEE1 transcript levels were significantly elevated in SCNPC over ARPC in three previously published datasets (Figure 2.5B-D). WEE1 expression is positively correlated with NE-signature score and negatively correlated with AR-signature score in our patient dataset (Figure 2.5E, F). This trend in WEE1 expression was also observed in prostate PDX models (Figure 2.5G-I). At the protein level, I determined that WEE1 is highly expressed in SCNPC cell lines and PDX models, although it can be similarly expressed in some ARPC models (Figure 2.5 J, K). Further examination of WEE1 protein in the LuCaP PDX models by IHC revealed that WEE1 staining intensity was generally elevated in SCNPC models compared to ARPC models (Figure 2.5L, M).

2.4.6 ABT-263 and AZD-1775 act synergistically to reduce viability in SCNPC cell lines

Dose response curves with the WEE1 inhibitor, AZD-1775, revealed that the compound had minimal effects on the viability of SCNPC cell lines (NCI-H660, MSKCC EF1), but resulted in a substantial reduction in the viability of several ARPC lines (LNCaP, C4-2, LAPC4, VCaP) at nanomolar concentrations (Figure 2.6A).

I next tested combinations of ABT-263 and AZD-1775 in two ARPC cell lines, LNCaP and C4-2, and two SCNPC cell lines, NCI-H600 and MSKCC EF1 (Figure 2.6B-E). Based on dose-response curves alone, SCNPC lines are more sensitive to lower doses of the combinations of AZD-1775 and ABT-263 than ARPC lines. To determine whether these inhibitors have additive or synergistic effects in the cell lines assayed, I used two analysis methods: isobologram analysis [77] and the Combination Index (CI) method [78] (Figure 2.6F-I). Consistent with synergy, the doses of AZD-1775 necessary to achieve a given IC value in the presence of ABT-263 were lower than those on the corresponding line of Loewe additivity for the SCNPC NCI-H660 line, but not the ARPC C4-2 line (Figure 2.6F, H, respectively). In addition, calculated CI values for NCI-H660 treated with the combination were less than one at several IC levels, indicating synergy (Figure 2.6G), while CI values for C4-2 suggest possible antagonism of the inhibitors in this cell line (Figure 2.6I).

"On-target" WEE1 inhibition of AZD-1775 was confirmed by Western Blot for the WEE1-mediated phosphorylation of CDK1 at tyrosine 15 in selected cell lines (Figure 2.6J). Phosphorylation of BCL2 at serine 70 by CDK1 has been noted to occur during prolonged mitosis and inhibits the anti-apoptotic activity of BCL2 [79, 80]. After treatment with AZD-

1775, p-BCL2 (s70) levels increased in the NCI-H660 line, indicating an increase in "inactive" BCL2 (Figure 2.6J).

2.4.7 ABT-263 and AZD-1775 have additive or synergistic effect on reducing growth in SCNPC PDX models

In collaboration with Dr. Eva Corey at the University of Washington, we treated SCNPC PDX models with the BCL2 inhibitor, ABT-263, and the WEE1 inhibitor, AZD-1775, singly or in combination (Figure 2.7A). LuCaP 49 and LuCaP 173.1, the same models that displayed reduced growth after treatment with ABT-263, also exhibited reduced growth after treatment with AZD-1775. Notably, four out of five models showed reduced growth when treated with the combination of ABT-263 and AZD-1775. LuCaP 93, a model resistant to ABT-263 or AZD-1775 single agent treatment, achieved an average end of study tumor volume four times smaller with the drug combination compared to vehicle treated tumors.

To confirm "on-target" activity of the WEE1 inhibitor, AZD-1775, in the PDX tumors, we performed IHC for a WEE1 mediated-phosphorylation on CDK1 at tyrosine 15 in tumors from this study (Figure 2.7B). Consistent with WEE1 inhibition, phospho-CDK1 levels were decreased in tumors that were treated with AZD-1775. Dissociation and *in vitro* treatment of the SCNPC PDX model LuCaP 49 with ABT-263 and/or AZD-1775 also led to a decrease in phospho-CDK1(Y15) levels and the combination treatment resulted in elevated cleaved caspase-3 over vehicle treated dissociated cells (Figure 2.7C).

2.5 Discussion

The aggressive clinical course and limited therapeutic options make SCNPC a subtype with shortened survival. In this study I identified BCL2 as highly expressed in SCNPC patient

metastases, PDX models, and cell lines. While inhibitors to BCL2 showed promise in reducing the viability of SCNPC cell lines, the response was heterogeneous in PDX models. A mechanistic understanding of the variable response to BCL2 antagonism remains lacking. Seeking additional therapeutic targets to evaluate in combination with BCL2 in SCNPC, we identified WEE1. In this study I presented data demonstrating the efficacy of dual BCL2 and WEE1 inhibition in pre-clinical models of SCNPC.

High BCL2 expression has long been reported in neuroendocrine tumor types [68, 81]. A hypothesis to explain elevated BCL2 expression in neuroendocrine tumors has been appropriated from the study of lymphomas-- that MYC amplification necessitates the amplification of anti-apoptotic proteins to overcome apoptotic cues induced by oncogenic stress (i.e. MYC overexpression leads to upregulation of the pro-apoptotic protein BIM, which can be sequestered by BCL2) [82, 83]. In the case of neuroblastoma, MYCN amplification has been noted to occur in conjunction with BCL2 overexpression or amplification [81].

Another mechanism that may promote high BCL2 expression in some SCNTs may be transcriptional activation by ASCL1. In SCLC, BCL2 has been identified as a direct target of ASCL1 [84]. High expression of ASCL1 has also been observed in SCNPC [85], but expression is rare in MCC, with a previous study identifying ASCL1 staining in 1/28 biopsies assayed [86]. Further work is necessary to characterize the diversity of mechanisms that promotes high BCL2 expression in SCNTs.

Recent work has shown that BCL2 inhibitors induce apoptotic cell death in SCLC and MCC cell lines [57, 58]. Clinical trials with BCL2 inhibitors have shown efficacy in leukemias and some solid tumors but have been plagued by toxicities due to concurrent inhibition of BCLXL, which has roles in platelet maintenance [87]. The BCL2 inhibitor ABT-199, also

named Venetoclax, was recently approved by the FDA for the treatment of Chronic Lymphocytic Leukemia and Acute Myeloid Leukemia owing to its efficacy and tolerability. However, recent reports indicate that resistance can rapidly develop in patients through the upregulation of other anti-apoptotic proteins with similar binding profiles to BCL2, such as MCL1 [88]. One method to potentiate the therapeutic efficacy of BCL2 inhibitors may be to administer them concurrently with another targeted agent, as many trials are now investigating. For this reason, I identified WEE1 kinase as a candidate for study in combination with BCL2 inhibition.

Although the combination of BCL2 and WEE1 inhibition is novel, it has previously been proposed that BCL2 family proteins can regulate sensitivity to antimitotic agents [89, 90]. CDK1, negatively regulated by WEE1, phosphorylates and inactivates anti-apoptotic BCL2 family members, including BCL2, during prolonged mitosis leading to cell death [80, 91]. A recent study has also suggested that DNA damage induced by AZD-1775 can enhance the dependency of diffuse large B-cell lymphoma on anti-apoptotic proteins, including BCL2, for survival [57]. Additional studies will be necessary to determine whether the mechanism of synergy between ABT-263 and AZD-1775 is solely mediated by inactivation of BCL2.

2.6 Figures

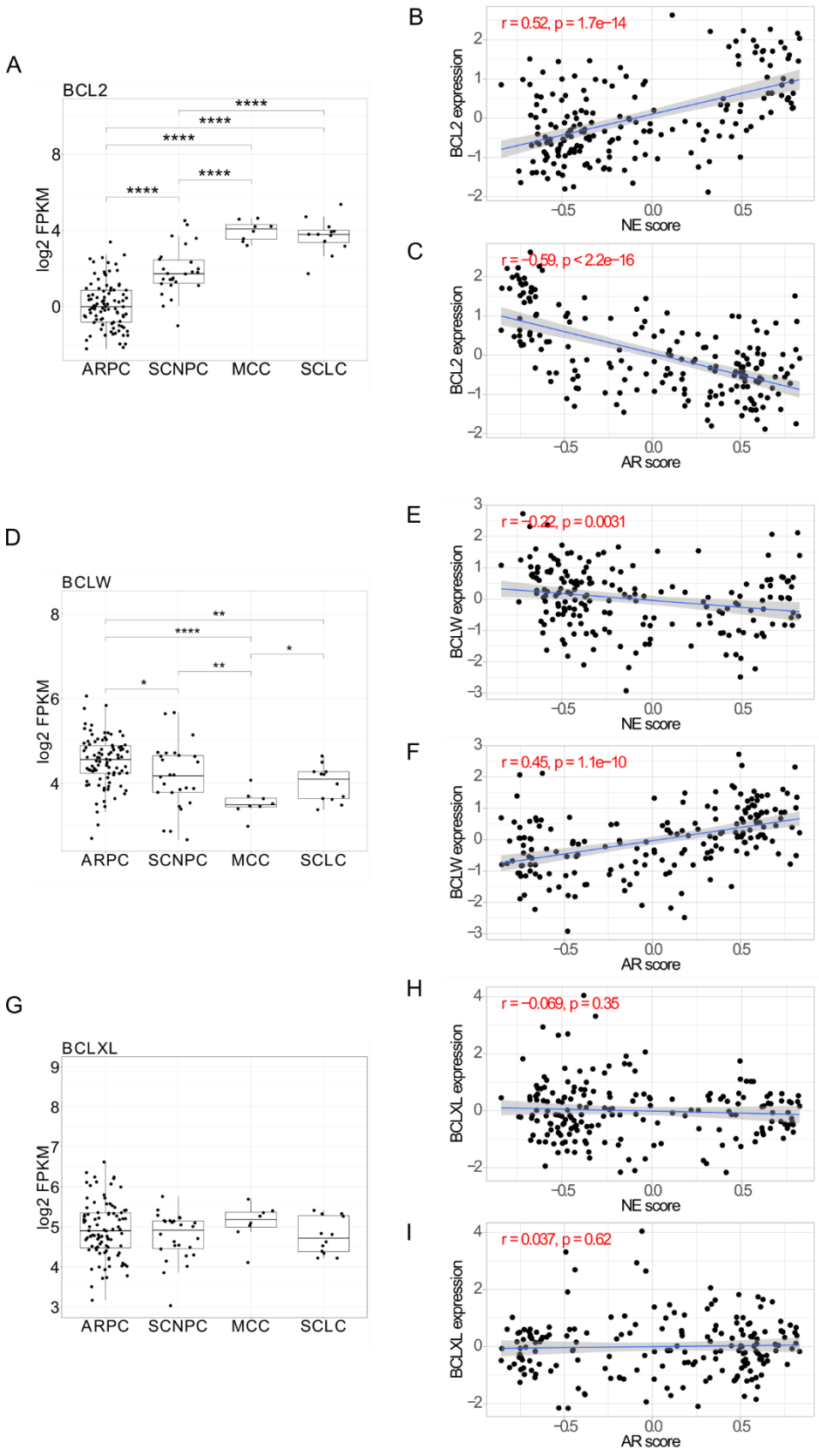
A
BCL2
log2 FPKM
ARPC
SCNPC
MCC
SCLC
B
r = 0.52, p = 1.7e−14
BCL2 expression
NE score
C
r = −0.59, p < 2.2e−16
BCL2 expression
AR score
D
BCLW
log2 FPKM
ARPC
SCNPC
MCC
SCLC
E
r = −0.22, p = 0.0031
BCLW expression
NE score
F
r = 0.45, p = 1.1e−10
BCLW expression
AR score
G
BCLXL
log2 FPKM
ARPC
SCNPC
MCC
SCLC
H
r = −0.069, p = 0.35
BCLXL expression
NE score
I
r = 0.037, p = 0.62
BCLXL expression
AR score

Figure 2.1 BCL2, but not BCLW or BCLXL, is highly expressed in SCNPC patient metastases. (**A**) Boxplot of BCL2 expression across tumor subtypes determined by RNA-sequencing. (**B, C**) Scatterplots of BCL2 expression with AR-signature or NE-signature score (r= Pearson correlation). (**D**) Boxplot of BCLW expression across tumor subtypes determined by RNA-sequencing. (**E, F**) Scatterplots of BCLW expression with AR-signature or NE-signature score. (**G**) Boxplot of BCLXL expression across tumor subtypes determined by RNA-sequencing. (**H, I**) Scatterplots of BCLXL expression with AR-signature or NE-signature score. * indicates $p \leq 0.05$, ** = $p \leq 0.01$, *** = $p \leq 0.001$, **** = $p \leq 0.0001$ by Student's t-test.

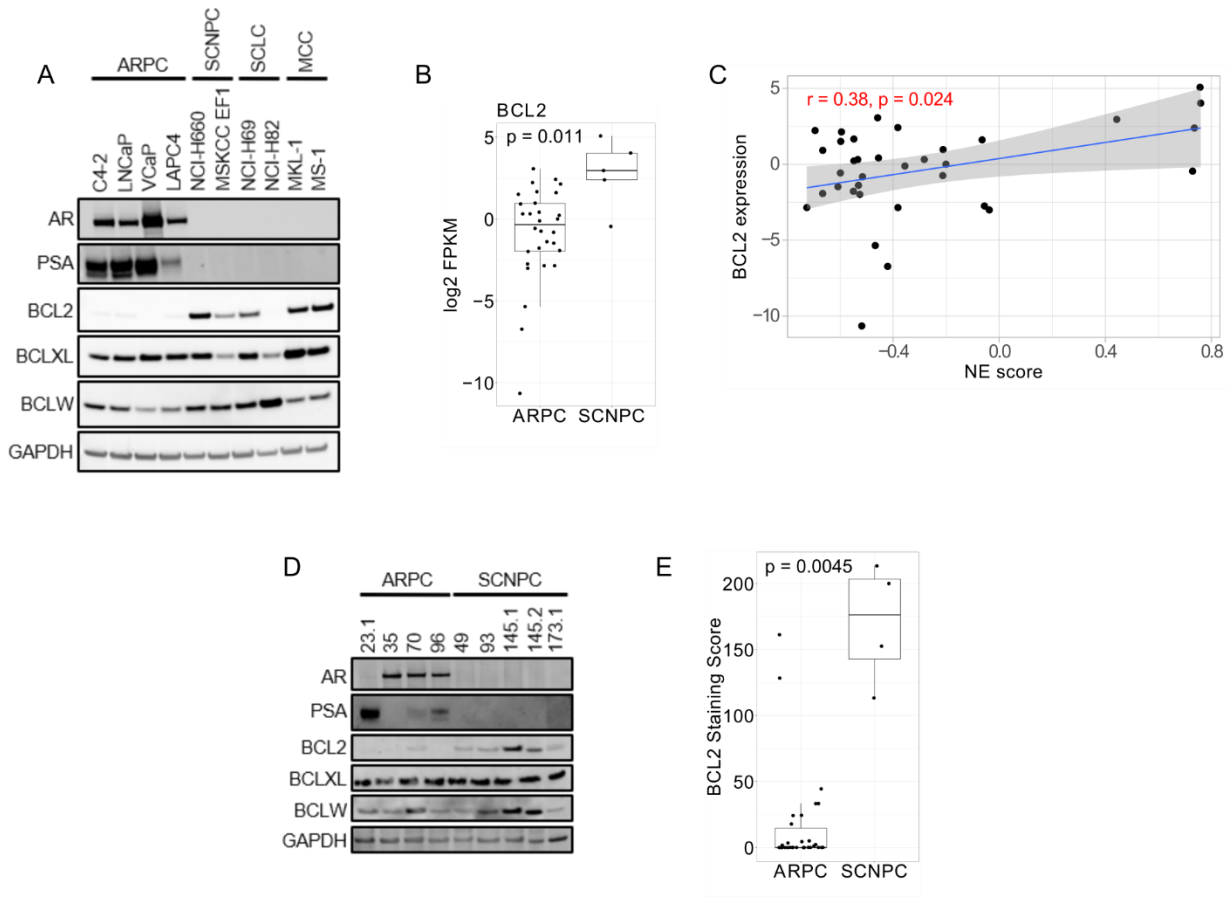

Figure 2.2 BCL2, but not BCLW or BCLXL, is highly expressed in SCNPC cell lines and PDX models. (**A**) Western Blot for indicated proteins across a panel of cell lines. (**B**) Boxplot depicting BCL2 expression across prostate cancer PDX models measured by RNA-sequencing. (**C**) Scatterplot of BCL2 expression and NE-signature score in prostate cancer PDX models (r = Pearson correlation). **(D**) Western Blot for indicated proteins across a panel of prostate PDX models. (**E**) Boxplot summarizing BCL2 expression as assessed by IHC. p indicates result of Student's t-test.

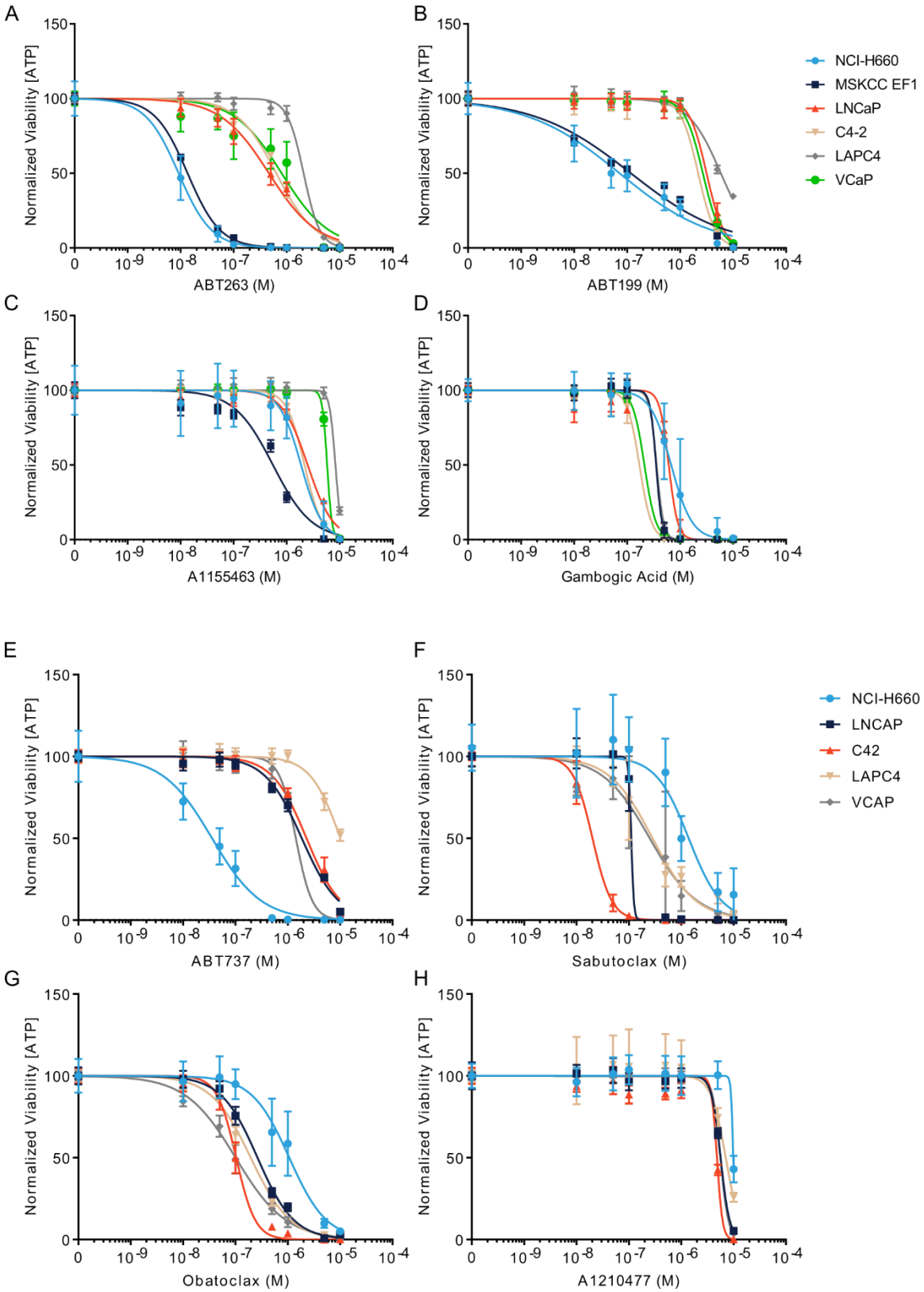
A
B
C
D
E
F
G
H
Normalized Viability [ATP]
ABT263 (M)
ABT199 (M)
A1155463 (M)
Gambogic Acid (M)
ABT737 (M)
Sabutoclax (M)
Obatoclax (M)
A1210477 (M)
NCI-H660
MSKCC EF1
LNCaP
C4-2
LAPC4
VCaP
NCI-H660
LNCAP
C42
LAPC4
VCAP

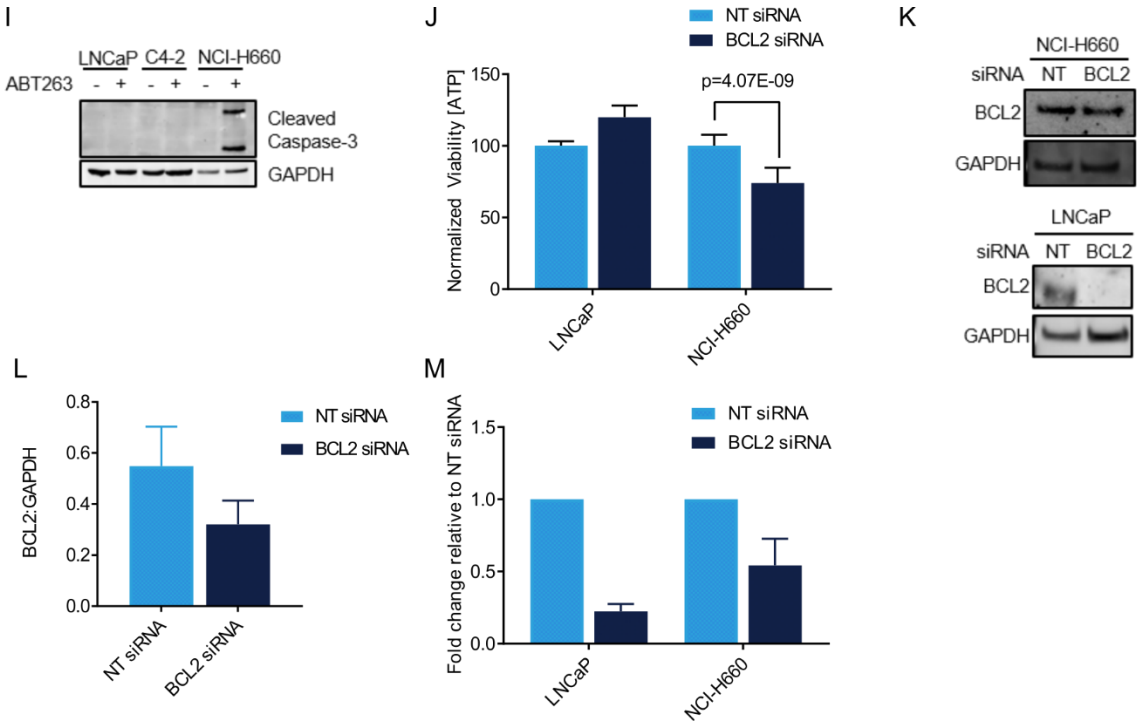

Figure 2.3 Viability of SCNPC cell lines is decreased by BCL2 inhibition. (**A-H**) Dose-response curves for drug indicated in a panel of cell lines (NCI-H660, MSKCC EF1 represent SCNPC, LNCaP, C4-2, LAPC4, VCaP represent ARPC). (**I**) Western Blot for cleaved caspase-3 following 24-hour treatment with 100 nM ABT-263 of cell line indicated. (**J**) Viability of cell line indicated assayed 96-hours post transfection with BCL2 siRNA or a non-targeting (NT) siRNA. (**K**) Western Blot for BCL2 with lysates collected 96-hours post-transfection of indicated siRNA. (**L**) Bar plot of average Western Blot band intensity collected from three independent siRNA experiments. (**M**) Bar plot of fold change measured by qPCR for BCL2 in cell line indicated for siRNA indicated. Error bars represent standard deviation.

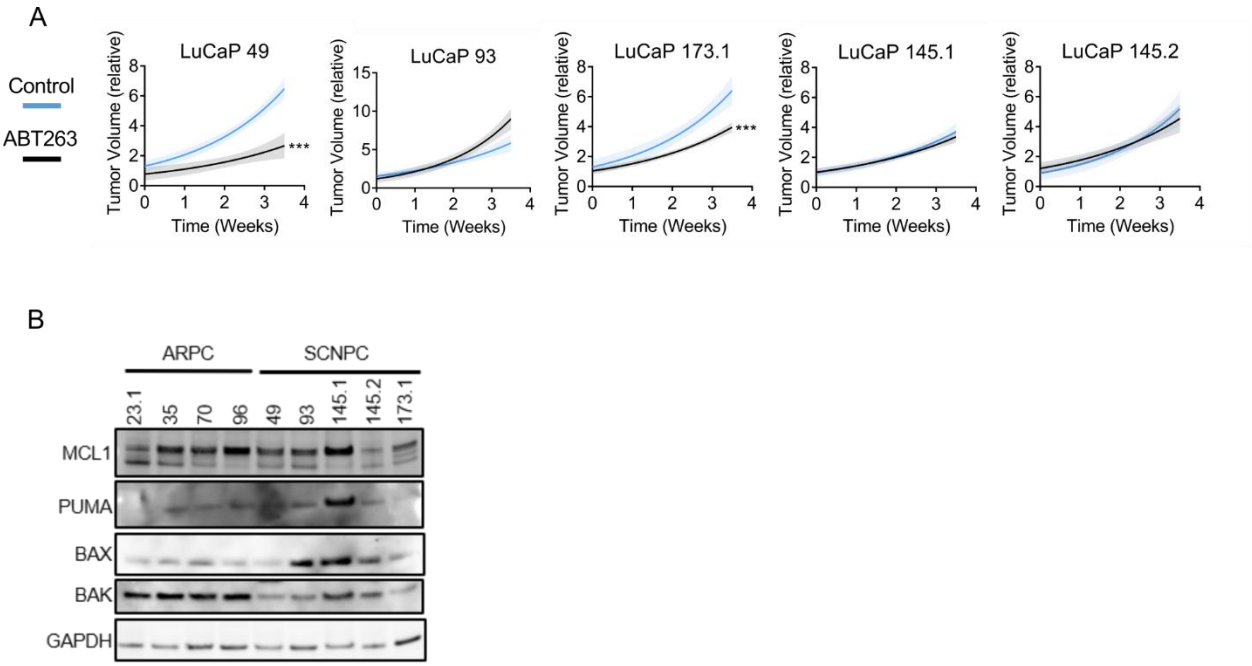

Figure 2.4 BCL2 inhibition decreases growth of some SCNPC models. (**A**) Normalized tumor volumes of SCNPC PDX models treated with vehicle control or ABT-263, *** indicates $p<0.05$. (**B**) Western Blot depicting expression of additional BCL2 family members in prostate cancer PDX models.

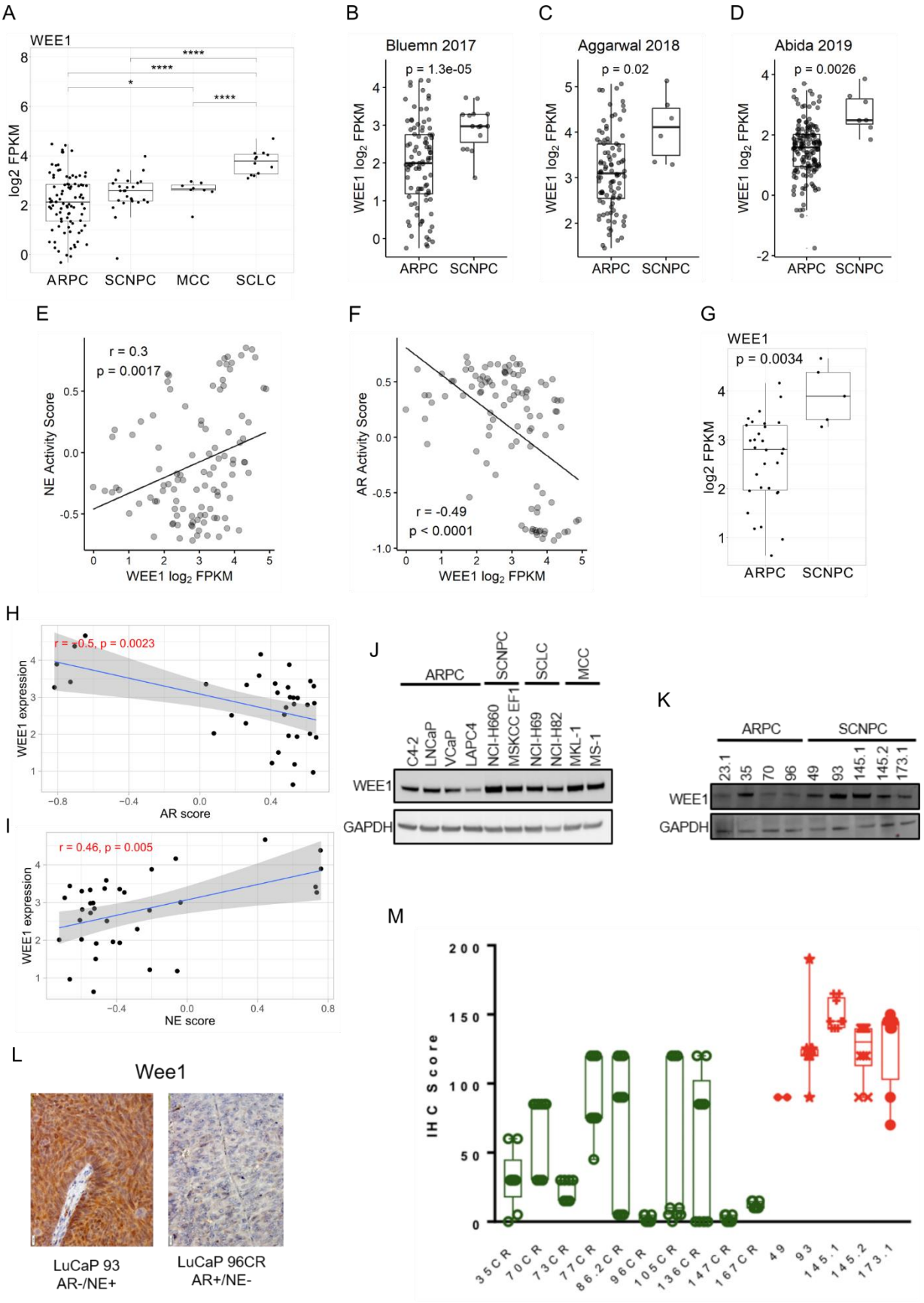
A
WEE1
log2 FPKM
ARPC
SCNPC
MCC
SCLC
B
Bluemn 2017
p = 1.3e-05
WEE1 log2 FPKM
C
Aggarwal 2018
p = 0.02
D
Abida 2019
p = 0.0026
E
r = 0.3
p = 0.0017
NE Activity Score
WEE1 log2 FPKM
F
AR Activity Score
r = -0.49
p < 0.0001
G
WEE1
p = 0.0034
H
r = -0.5, p = 0.0023
WEE1 expression
AR score
I
r = 0.46, p = 0.005
NE score
J
ARPC
SCNPC
SCLC
MCC
C4-2
LNCaP
VCaP
LAPC4
NCI-H660
MSKCC EF1
NCI-H69
NCI-H82
MKL-1
MS-1
WEE1
GAPDH
K
ARPC
SCNPC
23.1
35
70
96
49
93
145.1
145.2
173.1
WEE1
GAPDH
L
Wee1
LuCaP 93
AR-/NE+
LuCaP 96CR
AR+/NE-
M
IHC Score
35CR
70CR
73CR
77CR
86.2CR
96CR
105CR
136CR
147CR
167CR
49
93
145.1
145.2
173.1

Figure 2.5 WEE1 is highly expressed in SCNPC. (**A**) Boxplot of expression WEE1 across patient metastases as measured by RNA-sequencing, * indicates $p \leq 0.05$, **** = $p \leq 0.0001$ by Student's t-test. (**B-D**) Boxplots depicting WEE1 transcript levels measured by RNA-sequencing in three published studies. (**E, F**) Scatterplots of WEE1 expression and NE- or AR-signature score in patient metastases. (**G**) Boxplot of WEE1 expression across prostate cancer PDX models as measured by RNA-sequencing. (**H, I**) Scatterplots of WEE1 expression and NE- or AR-signature in prostate cancer PDX models. (**J, K**) Western Blots depicting WEE1 protein expression across a panel of cell lines and prostate cancer PDX models, respectively. (**L**) Representative images of WEE1 IHC in an SCNPC (LuCaP 93) and an ARPC (LuCaP 96CR) PDX model. (**M**) Boxplots of IHC staining score for WEE1 across a panel of prostate cancer PDX models (green represents ARPC, red represents SCNPC PDX models).

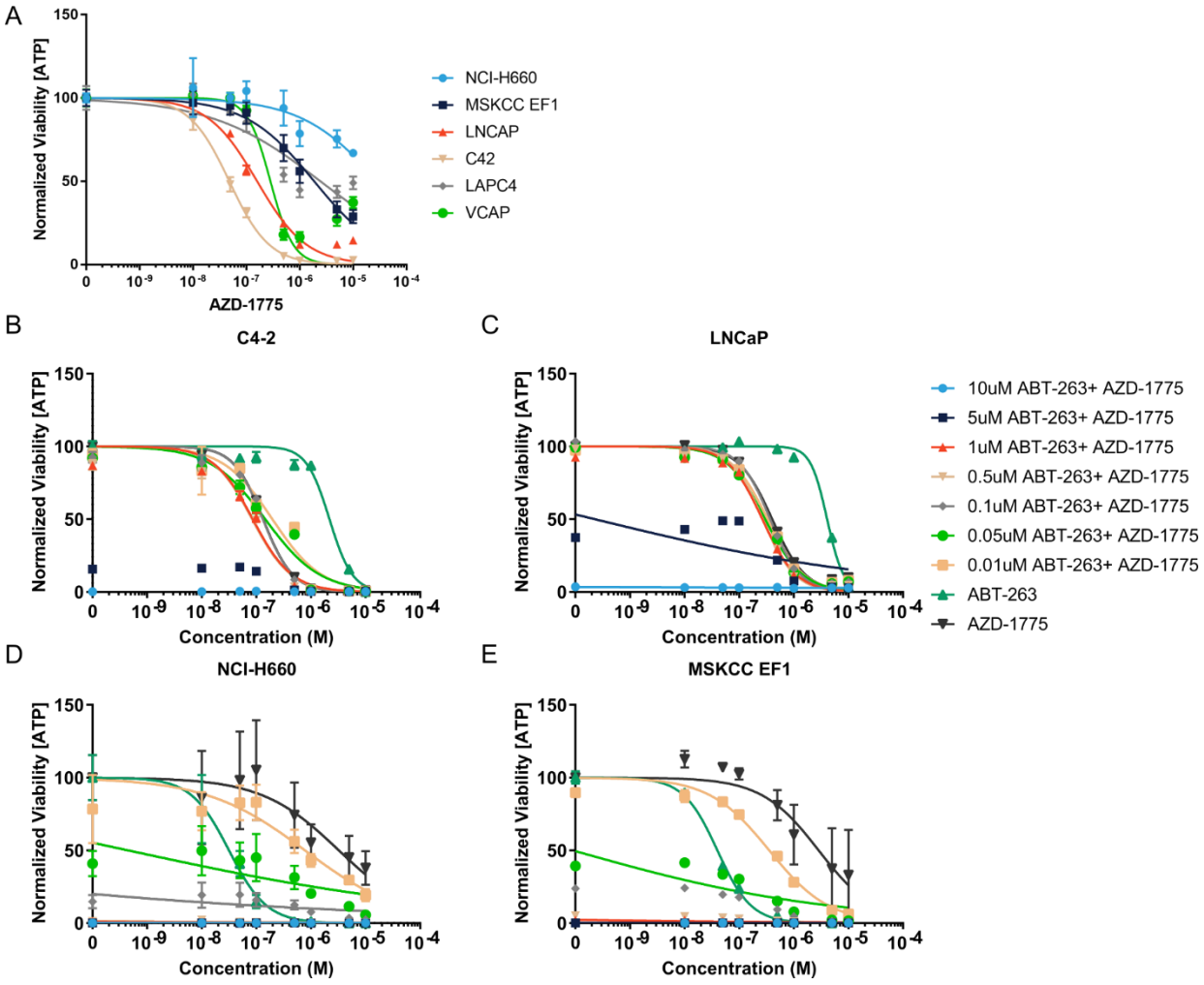
A
Normalized Viability [ATP]
AZD-1775
NCI-H660
MSKCC EF1
LNCAP
C42
LAPC4
VCAP
B
C4-2
C
LNCaP
Concentration (M)
10uM ABT-263+ AZD-1775
5uM ABT-263+ AZD-1775
1uM ABT-263+ AZD-1775
0.5uM ABT-263+ AZD-1775
0.1uM ABT-263+ AZD-1775
0.05uM ABT-263+ AZD-1775
0.01uM ABT-263+ AZD-1775
ABT-263
AZD-1775
D
NCI-H660
E
MSKCC EF1

F

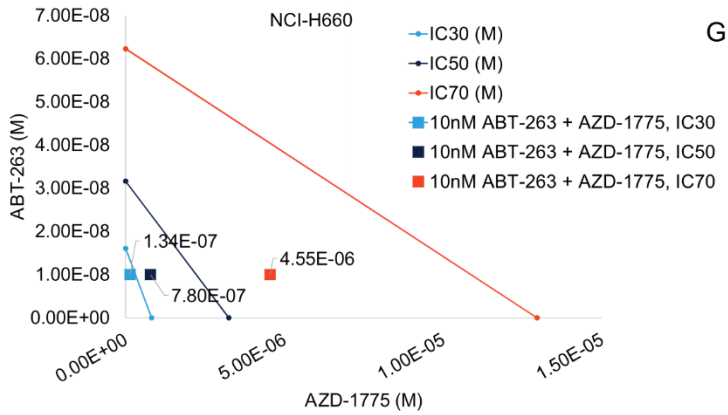

G

10nM ABT-263 + AZD-1775 in NCI-H660			
IC	ABT-263	AZD-1775	CI
30	1.00E-08	1.34E-07	0.786
50	1.00E-08	7.80E-07	0.556
70	1.00E-08	4.55E-06	0.512

H

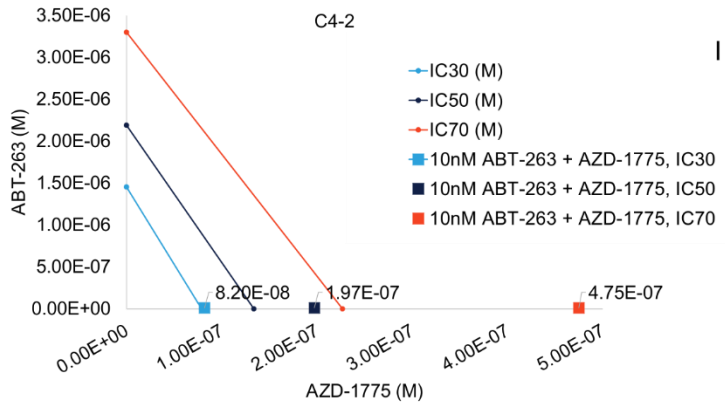

I

10nM ABT-263 + AZD-1775 in C4-2			
IC	ABT-263	AZD-1775	CI
30	1.00E-08	8.20E-08	1.047
50	1.00E-08	1.97E-07	1.480
70	1.00E-08	4.75E-07	2.097

J

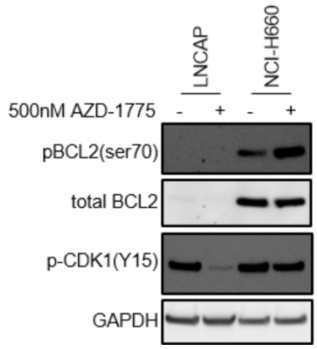

Figure 2.6 ABT-263 and ABT-199 combination studies in cell lines. (**A**) Dose-response curves depicting response to the WEE1 inhibitor, AZD-1775. (**B-E**) Viability of SCNPC (NCI-H660, MSKCC EF1) and ARPC cell lines (LNCaP, C4-2) following treatment with ABT-263, AZD-1775, or the combination. X-axis represents concentration of inhibitor when not indicated in legend. (**F**) Isobologram of ABT-263 and AZD-1775 in NCI-H660. (**G**) Chart showing ICs of AZD-1775 with 10 nM ABT-263 and combination index scores. (**H**) Isobologram of ABT-263 and AZD-1775 in C4-2. (**I**) Chart showing ICs of AZD-1775 in with 10 nM ABT-263 and combination index scores. (**J**) Western Blot of cell line indicated with or without 500 nM AZD-1775.

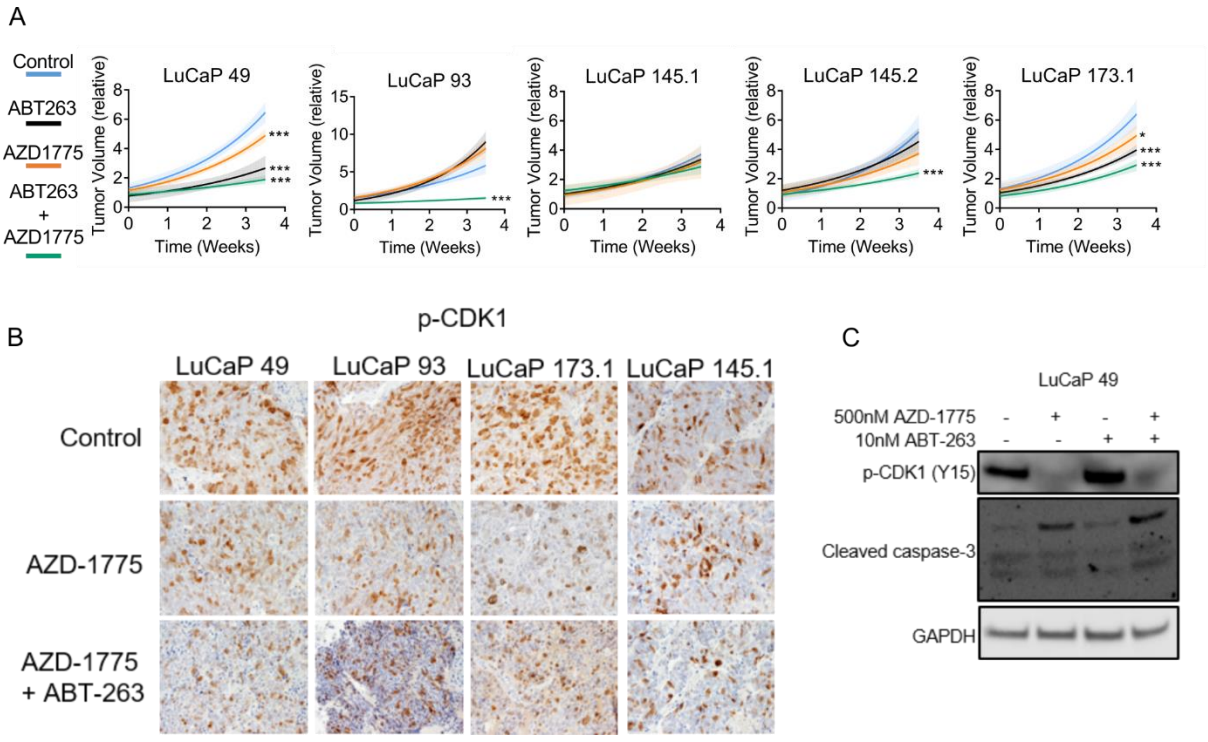

Figure 2.7 ABT-263 and AZD-1775 combination treatment in SCNPC PDX models. (**A**) Normalized tumor volumes of PDX models treated with vehicle control, ABT-263, AZD-1775 or the combination of ABT-263 and AZD-1775 or vehicle (bottom). *p<0.05; ***p<0.001. (**B**) Immunohistochemistry for p-CDK1 in four LuCaP SCNPC PDX lines treated *in vivo* with vehicle control, the Wee1 inhibitor AZD-1775 or the combination of AZD-1775 and the BCL2 inhibitor ABT-263. (**C**) Western blot for p-CDK1 and the apoptosis marker cleaved caspase-3 in dissociated cells from the LuCaP 49 SCNPC PDX model.

Chapter 3. INSM1 can promote neuroendocrine gene expression in prostate cancer

3.1 Abstract

The protein encoded by the insulinoma-associated 1 gene (INSM1) is a selective marker for many carcinomas exhibiting neuroendocrine features. It is known to play critical roles in the normal development of neuronal and neuroendocrine cells in many organs. Here, we report that INSM1 is highly expressed in SCNPC and is positively correlated with a 10-gene neuroendocrine signature. Overexpression of INSM1 led to protein expression of neuroendocrine marker genes in some ARPC models. INSM1 overexpression led to a decrease in REST expression and INSM1 was determined to be bound at the REST promoter, suggesting a regulatory hierarchy influencing neuroendocrine differentiation in prostate cancer.

3.2 Introduction

The development of the neuroendocrine (NE) phenotype in prostate cancer is marked by the loss of RE-1 silencing factor (REST) activity, also known as Neural-restrictive silencing factor (NRSF) [92]. As its name implies, REST is a transcriptional repressor that binds to neural lineage genes and facilitates silencing through recruitment of histone deacetylases and methyltransferases [93, 94]. REST maintains the non-neural identity in stem cells and differentiated non-neural cells [95]. Identifying how REST activity is lost in prostate cancer would be a crucial step toward understanding the development of the neuroendocrine phenotype.

An alternatively spliced isoform of REST that lacks a repressor domain is expressed in differentiated neurons [96]. Splicing of this isoform of REST, termed REST4, is mediated by Ser/Arg Repetitive Matrix 4 (SRRM4) [97]. Recent studies in prostate cancer have identified that SRRM4 is active and can promote the neuroendocrine phenotype [98, 99]. Using a patient transcriptome dataset consisting of androgen receptor-dependent prostate cancer (ARPC) and small cell or neuroendocrine tumors (SCNTs), including small cell or neuroendocrine prostate cancer (SCNPC), I sought to identify additional candidates that may regulate REST.

One such candidate is *Insulinoma associated 1* or INSM1. INSM1 is an intronless gene discovered in an insulinoma cDNA subtraction library [100]. INSM1 is a zinc-finger containing transcriptional repressor with a neuroendocrine cell-specific expression pattern [101]. INSM1 is expressed at the onset of neuronal differentiation and subsequently decreases [102]. INSM1 is essential for the normal development of endocrine tissues, including pancreatic endocrine cells [102, 103]. Elevated INSM1 expression has been proposed as a selective marker to distinguish many neuroendocrine tumors, including retinoblastoma, medulloblastoma, small cell lung cancer, neuroblastoma, and Merkel Cell carcinoma [104-106].

Recent studies of the developing mouse brain have suggested that INSM1 can directly repress REST transcription [107]. Further studies in lung cancer cell lines have demonstrated that INSM1 can modulate the expression of neuroendocrine associated genes including transcription factors, such as ASCL1, that regulate the expression of neuroendocrine associated genes [108]. I identified that INSM1 expression is elevated in SCNPC and in the following studies sought to evaluate its potential role in the development of the neuroendocrine phenotype in prostate cancer.

3.3 Materials and Methods

Selected methods adapted from a previously published work:

Corella AN, Cabiliza Ordonio MVA, Coleman I, Lucas JM, Kaipainen A, Nguyen HM, Sondheim D, Brown LG, True LD, Lee JK, MacPherson D, Nghiem P, Gulati R, Morrissey C, Corey E, Nelson PS. Identification of Therapeutic Vulnerabilities in Small-cell Neuroendocrine Prostate Cancer. Clin Cancer Res. 2019 Dec 5. doi: 10.1158/1078-0432.CCR-19-0775.

Patient sample and RNA collection

Prostate cancer metastases were collected as part of the Prostate Cancer Donor Program at the University of Washington. The collection of samples and RNA isolation of UW prostate cancer samples was carried out as previously described [10]. Merkel cell carcinoma patient samples and RNA were collected as part of a previously published study [33]. SCLC patient samples were obtained through the Cooperative Human Tissue Network. Human samples were collected with permission of the Institutional Review Board. SCLC cell lines NCI-H1436, NCI-H1672, NCI-H1963, NCI-H2141, NCI-H2195, NCI-H735, NCI-H774 were obtained from ATCC. RNA from tumor samples and cell lines was extracted with TRIzol (Invitrogen).

RNA-sequencing library prep and read processing

The purity and concentration of RNA was assessed by Nanodrop (Thermo Fisher) and Agilent Bioanalyzer. One microgram of total RNA was used as input to either the Illumina Tru Seq RNA Library Kit v2 or the Illumina TruSeq Stranded mRNA Library prep kit and libraries were prepared and barcoded according to the manufacturer's protocol. Libraries were sequenced on the Illumina HiSeq 2500 generating either 50 or 75 base-pair paired end reads. Resulting

reads were mapped to the hg38 human genome with TopHat v2.0.14 and transcript abundance was measured using the R Bioconductor package Genomic Alignments v1.18.0. Sequencing reads from patient-derived xenograft libraries were aligned to both hg38 human and mm10 mouse genomes. Reads that aligned with higher specificity to the mouse genome were removed as described [5] and remaining reads were processed as indicated for patient samples and cell lines.

Statistical Analyses

Differential expression analyses of RNA-sequencing data were carried out using the Bioconductor package edgeR v3.24.2 with transcript abundances as input. An FDR threshold of <0.05 was used as a cut-off for differential expression assessment. Multi-dimensional scaling analysis was conducted with all measured genes as input to the R Bioconductor package limma v3.38.3.

Calculation of AR and NE signature scores were carried out using the Bioconductor package GSVA v1.30.0 using z-score normalized log2 FPKM values as input. Scatterplots were created using ggplot2 v3.1.0 and the Pearson correlation between gene and signature score was calculated using the ggpubr v0.2 stat.cor() function.

Boxplots for individual genes were created with ggplot2 v3.1.0 and statistical assessment between groups was assessed by Student's t-test using the ggpubr v0.2 stat_compare_means() function.

Guilt-by-association analysis was performed by calculating the Pearson correlation between the log2FPKM expression of the lncRNA with that of each protein coding gene across all samples. Absolute values of the Pearson correlations were sorted, and the top 1% most highly

correlated protein coding genes was used as input to identify enriched KEGG pathways with the gProfiler R package. Additional KEGG enrichment analysis was also performed with the gProfiler R package.

Cell Lines

The cell lines, LNCaP (ATCC), 22Rv1 (ATCC), LAPC4, 22PCEP, LNCaP-AR (gifts of Charles Sawyers), R1AD1 (gift of Scott Dehm), and NCI-H660 (ATCC) were maintained in a 37ºC incubator with 5% CO_2 and grown in medium supplemented with fetal bovine serum and other additives as recommended by ATCC or the cell line provider. STR genotyping was used to authenticate the lines and cells were confirmed to be myco-plasma free using the MycoAlert Detection Kit (Lonza, LT07-418).

INSM1 or GFP overexpressing lines were generated by lentiviral transduction of pLX304 containing GFP (addgene) or INSM1. The human INSM1 ORF was obtained from Origene (cat# RG215007). INSM1 was amplified out and cloned into pLX304 by Golden Gate cloning.

Protein isolation and immunoblotting

Cell lines were washed 1x with PBS prior to the addition of a cell lysis buffer (1.5M Urea, 1% SDS, 1% NP-40, 2% Tween20, 250 nM NaCl, PBS) supplemented with 1x phosphatase inhibitors (PhosStop, Roche Diagnostics) and a 1x protease inhibitor cocktail (Complete Mini, Roche Diagnostics). PDX tissues were pulverized in liquid nitrogen with a mortar and pestle prior to the addition of lysis buffer. Lysates were sonicated and then centrifuged to clear debris. Protein quantification was performed using the Pierce bicinchoninic acid assay (Thermo Scientific). Lysates were mixed with LDS sample buffer and Reducing

Agent (NuPage) and heated at 70ºC for 10 minutes. Lysates were run on a 4-12% NuPage Bis-Tris gel and protein was transferred to a nitrocellulose membrane in Tris/CAPS buffer using a semi-dry transfer apparatus. Membranes were blocked and incubated with antibody solutions in 5% milk powder in 1x PBS with 0.01% Tween. Primary antibodies targeting INSM1 (Santa Cruz Biotechnology, cat# sc-377428, 1:500), SYP (Santa Cruz Biotechnology, cat# sc-17750, 1:10,000), CHGA (Abcam, cat# ab15160, 1:500), REST (Millipore, cat# 07-579, 1:1000), and GAPDH (BioRad, hFAB Rhodamine, cat# 12004167, 1:5000) were used. Secondary antibodies used were Goat-anti-Rabbit (Goat anti-Rabbit IgG (H+L) Secondary Antibody, HRP cat# 31460, 1:5000) and Goat-anti-Mouse (BioRad, StarBright Blue 700 cat# 12004158, 1:5000). Blots were imaged using the ChemiDoc MP (BioRad).

Chromatin Immunoprecipitation

Chromatin Immunoprecipitation (ChIP) was conducted with the MagnaChIP A/G Chromatin Immunoprecipitation kit from Millipore (cat# 17-10085) according to the manufacturer's instructions. Antibodies against INSM1 (INSM1 A-8, Santa Cruz Biotechnology, sc-271408 X) or IgG (Millipore, 12-371) were used.

Quantitative polymerase chain reaction

RNA was prepared from cell lines using the QIAGEN RNeasy kit (cat# 74106). One microgram of RNA was used to make cDNA with the SuperScriptII Reverse Transcriptase (Invitrogen, cat# 18064-14), following the manufacturer's protocol. qPCR reactions were performed in triplicate on the QuantStudio5 Real-Time PCR Machine (Applied Biosystems)

using SYBR Green PCR master mix. qPCR reactions were prepared and run the same for ChIP-qPCR experiments, according to the Millipore's instructions.

PCR primers used were AR Fwd 5' ATCCTCATATGGCCCAGTGTCAAG3', AR Rev 5' GCTCTCTAAACTTCCCGTGGCATA3', PSA Fwd 5' GCATGGGATGGGGATGAAGTAAG3', PSA Rev 5' CATCAAATCTGAGGGTTGTCTGGA3', FKBP5 Fwd 5'AAAGGCCACCTAGCTTTTTGC3', FKBP5 Rev 5' CCCCCTGGTGAACCATAATACA3', REST Fwd 5' TGGAAAATGCAACTATTTTTCAGA3', REST Rev 5' GAACTTGAGTAAGGACAAAGTTCACA3', NCAM1 Fwd 5' GGCATTTACAAGTGTGTGGTTAC3', NCAM1 Rev 5' TTGGCGCATTCTTGAACATGA3', SYP Fwd 5'TGGTGTTCGGCTTCCTGAA3', SYP Rev 5' GCGGCCCAGCCTGTCT3', INSM1 Fwd 5' CCTCGCCTACCAATCTCTGC3', INSM1 Rev 5' TCCAGCAGTTCACAAGCCAT3', Insulin pro fwd 5'TGAGGAAGAGGTGCTGACGA3', Insulin pro rev 5'CCTCTTCTGATGCAGCCTGT3', REST pro fwd 1 5'GACTATGGGCTAGGCATTCC3', REST pro rev 1 5'GGAGGAATTACCCTCAGATGACAG3', REST pro fwd 1-2 5'CCGCTTGGTTATCCCGCTTC3', REST pro rev 1-2 5'GTAGCAGGTCATTGCTGAGCC3', REST pro fwd 2 5'CCGTCAAAGCCTGCGGATTC3', REST pro rev 2 5'CTACCAAGCAAGGAGTGCCC3', REST pro fwd 2-2 5'CTAAAGAGACCCGTCAAAGCCTG3', REST pro rev 2-2 (used with REST pro rev 2), REST pro fwd 3 5'GGGAGCCACTATGCTTCTGAGG3', REST pro rev 3 5'GGAATGCCTAGCCCATAGTC3', REST pro fwd 3-2

5’TACGACTGACGTTTAGGAAGG3’, REST pro rev 3-2

5’GATAACCAAGCGGAATGCCT3’.

Immunohistochemistry

LuCaP tissue microarrays (TMAs) were constructed as previously described [74]. The INSM1 antibody was obtained from Santa Cruz Biotechnology (cat# sc-271408) and was used according to the manufacturer’s instructions.

Rapid Immunoprecipitation Mass spectrometry of Endogenous proteins (RIME)

RIME was performed as previously described [109] using antibodies against INSM1 (INSM1 A-8, Santa Cruz Biotechnology, sc-271408 X) or IgG (Millipore, 12-371).

3.4 Results

3.4.1 INSM1 is highly expressed in SCNPC

Using whole-transcriptome RNA-sequencing data generated from patient metastases and cell lines, I identified INSM1 as highly upregulated in SCNPC and two other neuroendocrine tumor types, Merkel Cell carcinoma (MCC), and small cell lung cancer (SCLC) (Figure 3.1A). Consistent with this expression pattern, INSM1 RNA levels are positively correlated with a 10-gene neuroendocrine (NE) signature score and negatively correlated with a 10-gene androgen receptor (AR) activity score (Figure 3.1B,C) [10]. Analysis of exome data from a previously published study of 34 prostate cancer patients [22] revealed that INSM1 was amplified or highly expressed in 70% (7/10) of SCNPC tumors whereas amplification was only observed in 12.5% (3/24) of prostate adenocarcinomas (Figure 3.1D). Concurrent with the patient data, INSM1

protein was determined to be highly expressed in SCNPC patient-derived xenograft (PDX) models by Western Blot (Figure 3.1E) and IHC (Figure 3.1F,G). Western Blot analysis of a panel of prostate cancer and other SCNT cell lines demonstrated that INSM1 protein was present and elevated across SCNT cell lines, with the exception of the SCLC cell line NCI-H82 (Figure 3.1H). Low INSM1 expression has previously been noted in NCI-H82 [110].

3.4.2 INSM1 is sufficient to induce neuroendocrine gene expression in some models of ARPC

I overexpressed GFP or INSM1 in the prostate adenocarcinoma cell lines R1AD1, 22Rv1, 22PCEP, LAPC4, LNCaP-AR, LNCaP, and a previously characterized LNCaP clone (LNCaP B72) with *RB1* and *TP53* deleted by CRISPR [111]. INSM1 overexpression is sufficient to induce synaptophysin protein (SYP) expression in the R1AD1, 22PCEP, and LAPC4 cell lines that express no detectable SYP in cells transduced with GFP (Figure 3.2A). In the 22Rv1 model, an adenocarcinoma line that has strong basal levels of synaptophysin, INSM1 overexpression leads to an increase in the neuroendocrine marker chromogranin A (CHGA) (Figure 3.2A). INSM1 overexpression in LNCaP, LNCaP-AR, and LNCaP B72 did not lead to any detectable changes in neuroendocrine marker genes at the protein level (blots not shown). However, LNCaP cells overexpressing INSM1 did display an increase in some markers of neuroendocrine differentiation at the RNA level, as measured by qPCR (Figure 3.2B). Growing LNCaP cells in androgen-depleted serum, charcoal-stripped serum (CSS), may enhance the effect of INSM1 overexpression on some neuroendocrine marker transcription.

I profiled a subset of these GFP or INSM1 overexpressing cell lines by RNA-sequencing. INSM1 overexpression does not significantly alter expression of genes comprising the 10-gene

AR-signature score (Figure 3.2C, top) nor the expression of AR itself (Figure 3.2E). However, INSM1 can increase transcript levels of many genes comprising the NE-signature score in some cell line backgrounds (Figure 3.2C, bottom), including significant increases in SYP (Figure 3.2D) which may be attributable to increases in ASCL1 expression (Figure 3.2E). Co-expression of NE-signature and AR-signature genes have been found in many human CRPC samples that comprise the so-called "amphicrine" subtype generated by a loss of REST activity in tumors that maintain AR-signaling [112].

3.4.3 INSM1 overexpression induces heterogeneous transcriptional programs in ARPC models

Although INSM1 overexpression impacted the expression of thousands of genes in each individual ARPC line compared to GFP control, only 25 genes were determined to be differentially regulated (FDR<0.05, |log2 fold change|>2) across all INSM1 overexpressing lines profiled (Figure 3.3A). Among the genes induced by INSM1 overexpression in all models are several that have been previously associated with SCNPC, such as ESR1 and the neural lineage oncogene, ASCL1 [113, 114]. On a global level, INSM1 overexpression was not sufficient to overcome the intrinsic transcriptional programs of the cell lines profiled, as the majority of the lines cluster by cell type of origin and not GFP or INSM1 status (Figure 3.3B). However, Gene Set Enrichment Analysis (GSEA pre-ranked) with Hallmark gene sets indicates the activation of many pathways associated with the neuroendocrine phenotype and SCNTs, including significant enrichment in Hedgehog signaling (including upregulation of SHH, PTCH1, CDK6, HEY1, L1CAM, among others) and pancreatic beta cell gene sets (Figure3.3C,D, respectively). Of

interest, genes that contain REST (NRSF) binding site motifs were also significantly enriched across all INSM1 overexpressing lines (Figure 3.3E).

After separating the INSM1 overexpressing lines into two groups based on protein level expression of SYP or other neuroendocrine markers, many more transcriptional differences emerge. Placing 22Rv1, R1AD1, and LAPC4 overexpressing INSM1 in one group (NE-phenotype high) and LNCaP, LNCaP-AR, and LNCaP B72 (NE-phenotype low) in another, reveals alterations in the expression of over 1,300 genes (FDR<0.05, |log2 fold change|>2). Among these upregulated genes are CCND1, a known co-factor of INSM1, which facilitates its repressive function in neuronal/neuroendocrine development [115], and BCL2, which I associated with SCNPC in previous chapters. GSEA analysis reveals significant enrichment in Hallmark gene sets and KEGG pathways related to cell cycle, metabolism, and signaling pathways related to neuroendocrine tumors (Figure 3.3F, G).

3.4.4 INSM1 overexpression leads to lower REST levels in ARPC models

As REST is a major factor regulating the initiation of the neuroendocrine phenotype in prostate cancer, and the GSEA analysis revealed that expression of REST repressed genes was elevated in INSM1 overexpressing cell lines, I sought to further characterize the impact of INSM1 on REST expression. Western Blot analysis of cell lines with SYP-positive protein phenotypes induced by INSM1, indicate that REST protein is also decreased by INSM1 overexpression, compared to GFP controls (Figure 3.4A). REST expression is also decreased in the majority of INSM1 overexpressing cell lines, regardless of SYP expression, as assessed by RNA-sequencing (Figure 3.4B). As INSM1 is known to function as a transcriptional repressor, I hypothesize that it directly represses the transcription of REST. To begin to evaluate this

hypothesis, I used the JASPAR database of transcription factor binding sites [116], to search for INSM1 binding sites within 1000bp upstream of the REST transcriptional start site. JASPAR predicted 6 high confidence INSM1 binding sites in this region (Figure 3.4C). I next used ChIP-qPCR to evaluate whether INSM1 is present at three of the top scoring predicted binding sites with high scores in the REST promoter in the R1AD1 GFP, R1AD1 INSM1, and the SCNPC cell line, NCI-H660 (Figure 3.4D). A region of the insulin promoter previously described to be bound by INSM1 was used as a positive control [117]. Enrichment of INSM1 was observed at the three putative binding sites assessed in the REST promoter in R1AD1 INSM1 cells compared to R1AD1 GFP cells. These data support a mechanism by which INSM1 may directly regulate REST transcription.

3.4.5 INSM1 cofactors

Studies detailing the role of INSM1 in development have suggested that INSM1 requires cofactors, such as Cyclin D1, to recruit HDACs and facilitate silencing of its target genes [115]. Although no comprehensive studies have been conducted in SCNPC, Cyclin D1 is usually expressed at low levels, if at all in SCLC [27, 115]. Recent studies in SCLC and MCC have suggested that INSM1 plays a critical role in tethering the oncogene LSD1 to DNA and facilitating its silencing activity [118, 119]. To gain insight into how INSM1 may be regulating gene expression in prostate cancer, I performed Rapid Immunoprecipitation Mass spectrometry of Endogenous protein (RIME, [109]) on R1AD1 cells overexpressing INSM1 to identify factors with which INSM1 complexes on DNA. This approach utilizes a ChIP protocol followed by mass spectrometry to identify proteins that may be associated on chromatin with a protein of interest. Peptides corresponding to 465 proteins were identified as high confidence mass

spectrometry “hits” (FDR<0.01) in INSM1 samples after subtraction of all proteins identified in IgG controls. Of these 465 proteins, 154 were captured in both replicates (Figure 3.5A). As expected, the most confident protein identified after subtraction of those present in IgG controls is INSM1 itself. Of note, the SRRM family members, SRRM1 and SRRM2 and the neuro-specific splicing factor, NOVA1, were identified as high confidence INSM1-associated proteins. KDM1A, also known as LSD1, was also identified as a high confidence INSM1-associated protein. A recent study in MCC demonstrated that a complex consisting of LSD1, INSM1 and the REST co-repressors, RCOR1 and RCOR2, among other proteins is required for virus-mediated Merkel cell transformation [119]. The authors used a combination of ChIP-sequencing and RNA-sequencing to identify genes regulated by the LSD1 complex in MCC. I assessed the expression of this LSD1 MCC signature in the cell lines engineered for this study and found that it is generally elevated in INSM1 overexpressing lines compared to GFP controls (Figure 3.5B, C).

Overall, the 154 INSM1-associated proteins identified by RIME are enriched for pathways related to splicing, DNA repair, and ribosome biogenesis (Figure 3.5D). Additional studies are necessary to confirm the composition of INSM1 complexes and understand the functions of these complexes in regulating neuroendocrine differentiation.

3.5 Discussion

Although the functions of INSM1 in development have been extensively studied, its roles in SCNPC are not established. In this study, I provide evidence to suggest that INSM1 can facilitate the initiation of neuroendocrine gene expression in prostate cancer, possibly through the direct repression of REST.

While INSM1 overexpression only universally impacted the expression of 25 genes in the cell lines profiled, many of these have been associated with SCNPC. These genes include ASCL1, a lineage-specific transcription factor essential for the normal differentiation of many neuroendocrine cell types, including those in the lung [120]. ASCL1 expression is required for the proliferation of many small cell lung cancer models [121], making its downstream targets, which include BCL2, attractive drug targets [84].

I propose the model below, in which INSM1 expression leads to a decrease in the expression of REST, possibly through direct repression. The increase in ASCL1 expression seen in the majority of INSM1 overexpressing cell lines may be the direct result of the suppression of REST or it may be due to a yet unknown function of INSM1.

Recent studies have suggested that while the mutational landscapes of ARPC and SCNPC are largely similar, they have distinct epigenetic profiles [22]. One hypothesis as to why INSM1 overexpression induces a heterogeneous response in ARPC cell lines is that certain backgrounds may be more permissive, or perhaps "epigenetically" primed, for transdifferentiation, due to the presence of necessary co-factors or accessibility of target genes. Future studies incorporating chromatin accessibility, ChIP-sequencing, and the data generated in the present study may begin to address this hypothesis.

LSD1 has been reported to drive prostate cancer progression through a variety of mechanisms that include activity independent of its demethylase functions [122-125]. Pharmacologic or genetic inhibition of LSD1 reduces viability or proliferation in pre-clinical models of a variety of SCNTs, including in the SCNPC cell line NCI-H660 (from the project Achilles database, https://portals.broadinstitute.org/achilles) [126, 127]. The LSD1 inhibitor, GSK2879552, has been shown to reduce the viability of MCC cell lines through disruption of its

interaction with INSM1 [119]. Future studies into the role of INSM1 in the initiation or maintenance of SCNPC may focus on its connection to LSD1.

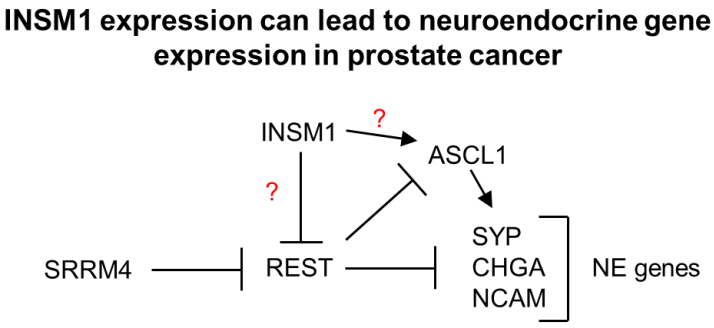

3.6 Figures

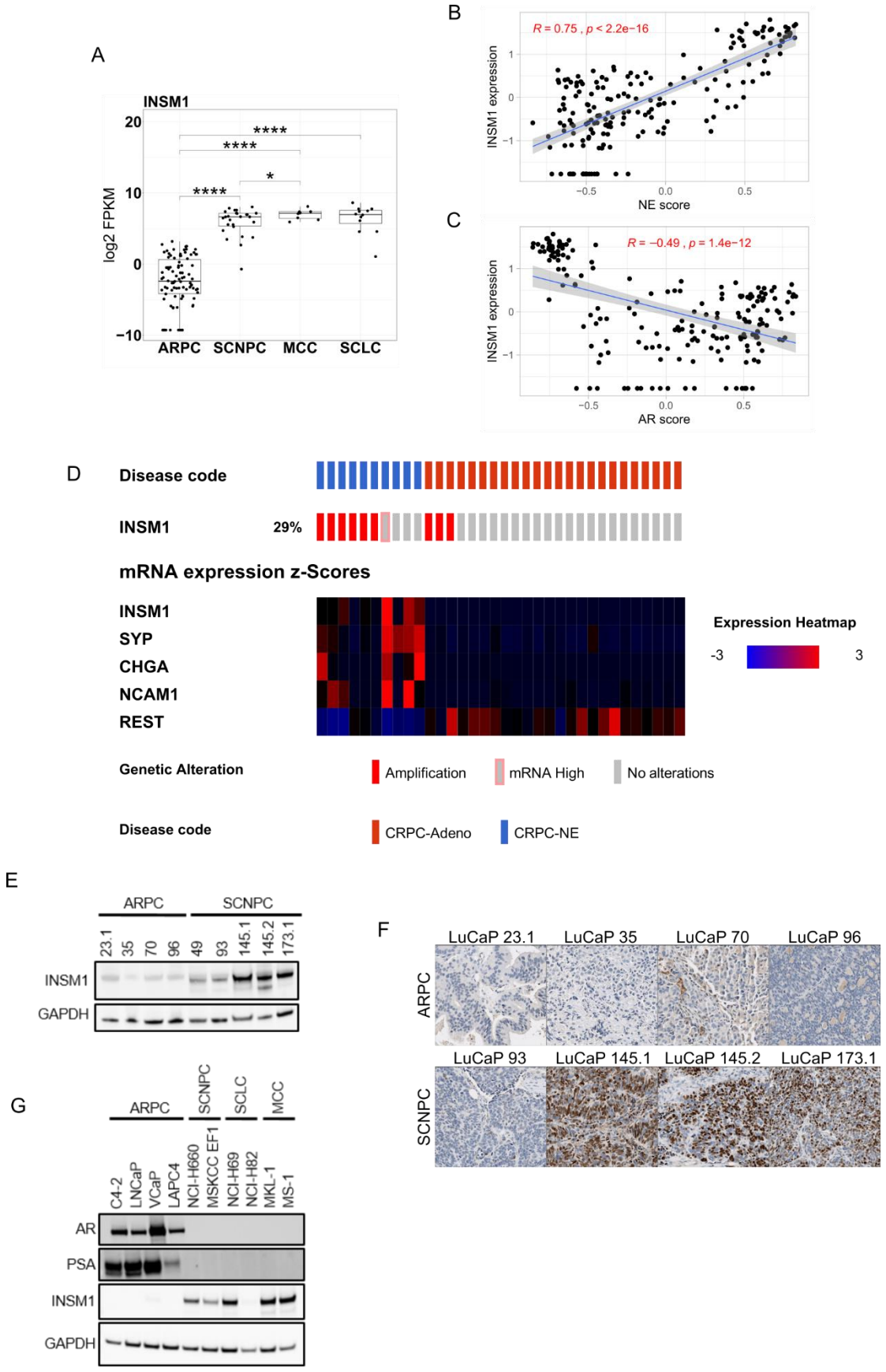
A
INSM1
log2 FPKM
ARPC
SCNPC
MCC
SCLC
B
R = 0.75 , p < 2.2e−16
INSM1 expression
NE score
C
R = −0.49 , p = 1.4e−12
INSM1 expression
AR score
D
Disease code
INSM1
29%
mRNA expression z-Scores
INSM1
SYP
CHGA
NCAM1
REST
Expression Heatmap
Genetic Alteration
Amplification
mRNA High
No alterations
Disease code
CRPC-Adeno
CRPC-NE
E
ARPC
SCNPC
23.1
35
70
96
49
93
145.1
145.2
173.1
INSM1
GAPDH
F
LuCaP 23.1
LuCaP 35
LuCaP 70
LuCaP 96
ARPC
LuCaP 93
LuCaP 145.1
LuCaP 145.2
LuCaP 173.1
SCNPC
G
ARPC
SCNPC
SCLC
MCC
C4-2
LNCaP
VCaP
LAPC4
NCI-H660
MSKCC EF1
NCI-H69
NCI-H82
MKL-1
MS-1
AR
PSA
INSM1
GAPDH

Figure 3.1 INSM1 is highly expressed in SCNPC. (**A**) Boxplot of INSM1 expression across patient metastases and cell lines. (**B,C**) Scatterplots of INSM1 expression and AR-signature or NE-signature score (r= Pearson correlation). (**D**) Heatmap summarizing INSM1 exome data and expression of selected genes. (**E**) Western Blot of INSM1 across prostate cancer PDX models. (**F**) Representative IHC images of INSM1 staining in prostate cancer PDX models. (**G**). Western Blot of INSM1 expression across a panel of cell lines. * indicates $p \leq 0.05$, **** = $p \leq 0.0001$ by Student's t-test.

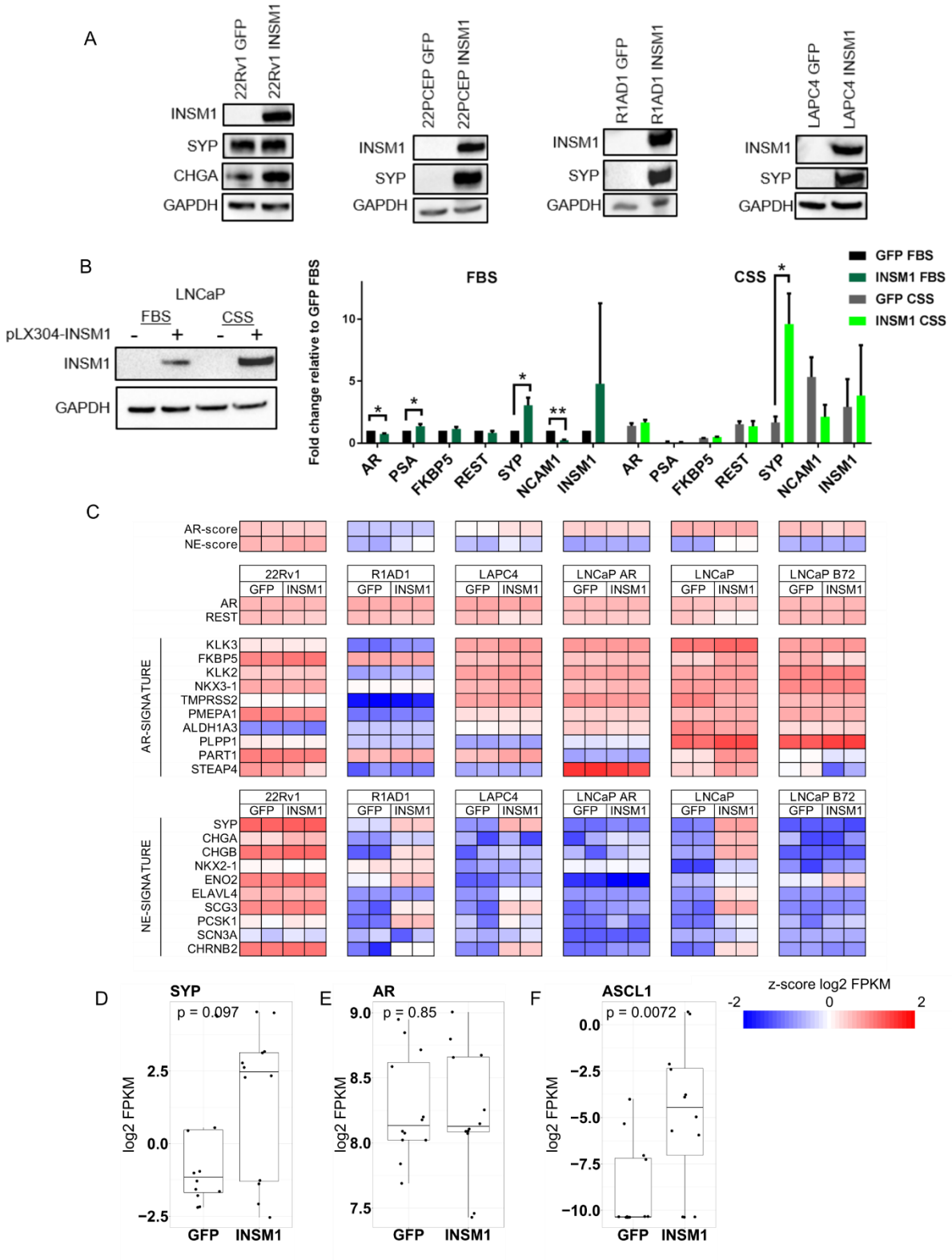
A
22Rv1 GFP
22Rv1 INSM1
22PCEP GFP
22PCEP INSM1
R1AD1 GFP
R1AD1 INSM1
LAPC4 GFP
LAPC4 INSM1
INSM1
SYP
CHGA
GAPDH
B
LNCaP
FBS
CSS
pLX304-INSM1
GFP FBS
INSM1 FBS
GFP CSS
INSM1 CSS
Fold change relative to GFP FBS
AR
PSA
FKBP5
REST
SYP
NCAM1
INSM1
C
AR-score
NE-score
22Rv1
R1AD1
LAPC4
LNCaP AR
LNCaP
LNCaP B72
GFP
INSM1
AR-SIGNATURE
KLK3
FKBP5
KLK2
NKX3-1
TMPRSS2
PMEPA1
ALDH1A3
PLPP1
PART1
STEAP4
NE-SIGNATURE
SYP
CHGA
CHGB
NKX2-1
ENO2
ELAVL4
SCG3
PCSK1
SCN3A
CHRNB2
z-score log2 FPKM
D
SYP
p = 0.097
log2 FPKM
E
AR
p = 0.85
F
ASCL1
p = 0.0072

Figure 3.2 INSM1 overexpression can induce neuroendocrine gene expression in some ARPC models. (**A**) Western Blots depicting indicated protein in GFP or INSM1 overexpressing cell lines. (**B**) Western Blot (left), and qPCR (right) for selected proteins and genes in GFP or INSM1 overexpressing LNCaPs grown in media containing FBS or charcoal-stripped serum (CSS). (**C**) Heatmap displaying expression of AR-signature or NE-signature genes in cell lines overexpressing GFP or INSM1. (**D-F**) Boxplots showing expression of indicated gene as measured by RNA-sequencing, p= Student's t-test.

A

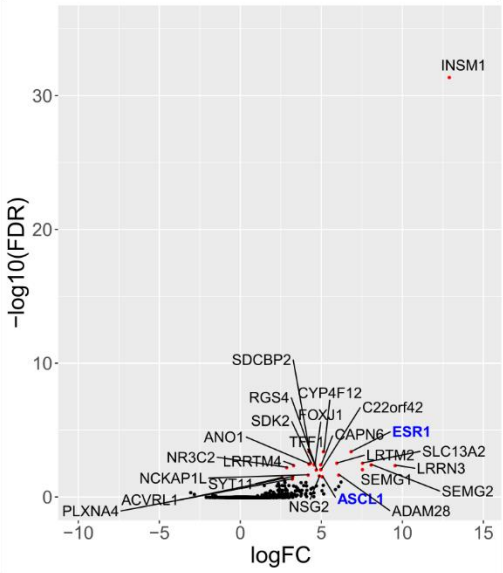
INSM1
SDCBP2
RGS4
CYP4F12
FOXJ1
C22orf42
SDK2
CAPN6
ESR1
ANO1
TFF1
LRTM2
SLC13A2
NR3C2
LRRTM4
LRRN3
NCKAP1L
SYT11
SEMG1
SEMG2
ACVRL1
ASCL1
NSG2
PLXNA4
ADAM28
−log10(FDR)
logFC

B

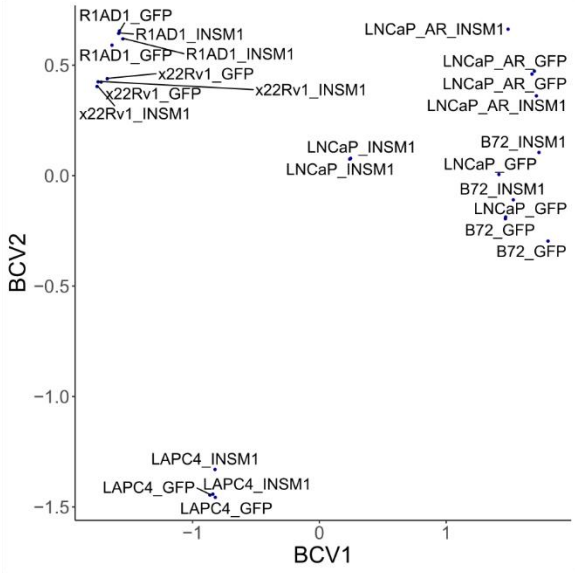
R1AD1_GFP
R1AD1_INSM1
LNCaP_AR_INSM1
LNCaP_AR_GFP
x22Rv1_GFP
x22Rv1_INSM1
LNCaP_INSM1
B72_INSM1
LNCaP_GFP
B72_GFP
LAPC4_INSM1
LAPC4_GFP
BCV2
BCV1

C

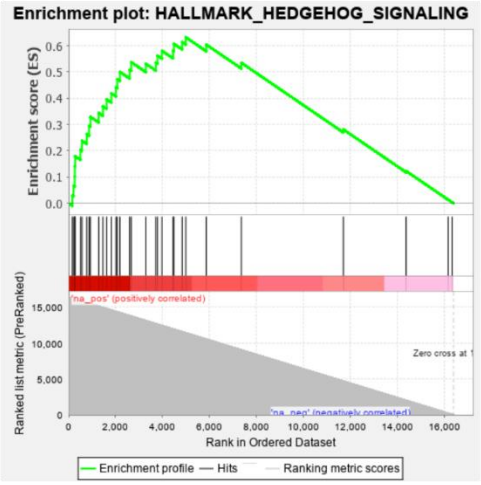
Enrichment plot: HALLMARK_HEDGEHOG_SIGNALING
Enrichment score (ES)
Ranked list metric (PreRanked)
Rank in Ordered Dataset
Enrichment profile
Hits
Ranking metric scores

D

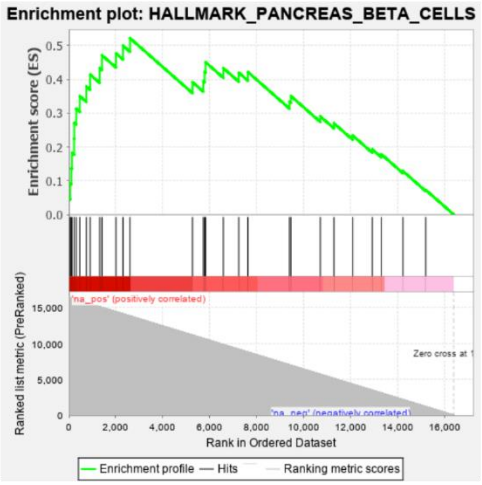
Enrichment plot: HALLMARK_PANCREAS_BETA_CELLS
Enrichment score (ES)
Ranked list metric (PreRanked)
Rank in Ordered Dataset
Enrichment profile
Hits
Ranking metric scores

E

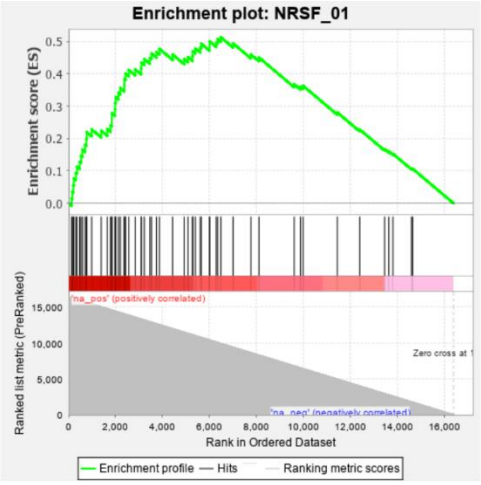
Enrichment plot: NRSF_01
Enrichment score (ES)
Ranked list metric (PreRanked)
Rank in Ordered Dataset
Enrichment profile
Hits
Ranking metric scores

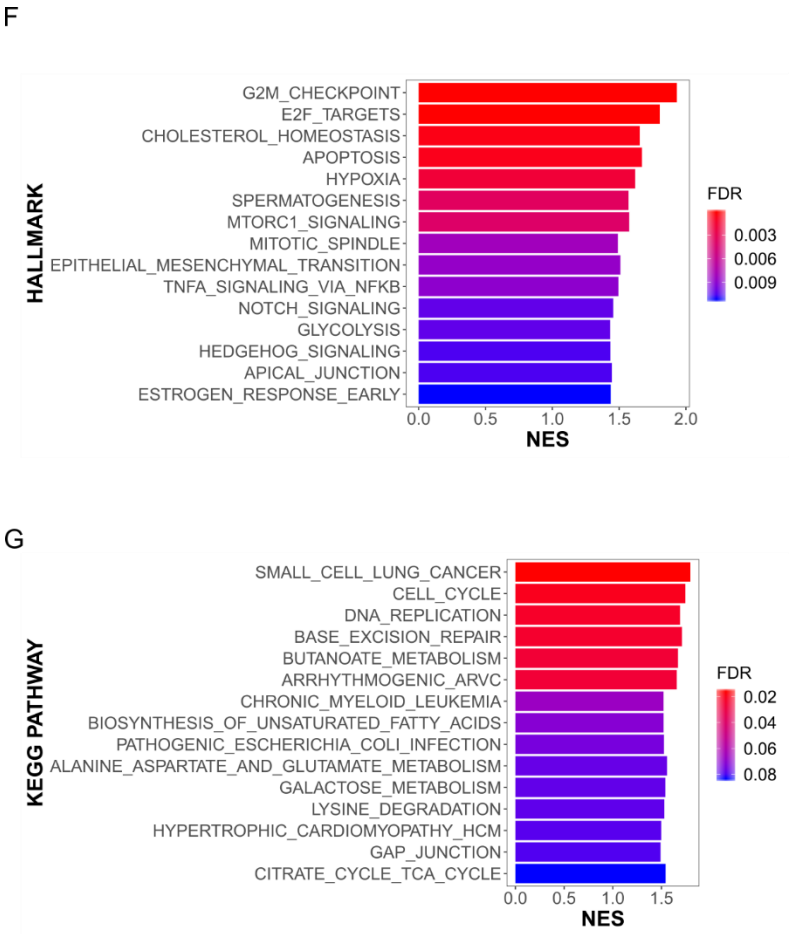

Figure 3.3 INSM1 induces a heteogeneous transcriptional response in ARPC lines. (**A**) Volcano plot of differentially expressed genes in all INSM1 lines compared to GFP controls. (**B**) Multi-dimensional scaling analysis of INSM1 or GFP overexpressing cell lines based on expression of all genes measured by RNA-sequencing. (**C-E**) GSEA plots for selected pathways or motifs. (**F,G**) Normalized Enrichment Scores (NES) for selected significantly enriched gene sets in INSM1 overexpressing lines that express SYP protein.

A

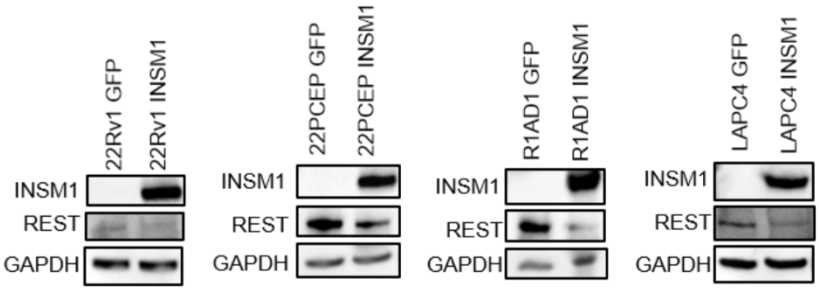

B

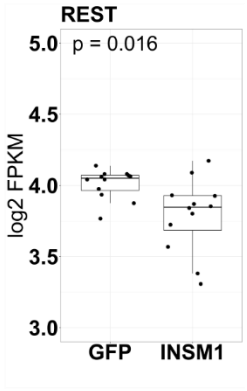

C

Score	Relative score	Start	End	Strand
12.7944	0.912378442	253	264	-
11.4026	0.883200252	825	836	-
10.8005	0.870576835	120	131	+
8.4053	0.820362295	812	823	-
8.31839	0.818540219	699	710	+
7.64465	0.80441567	784	795	+

D

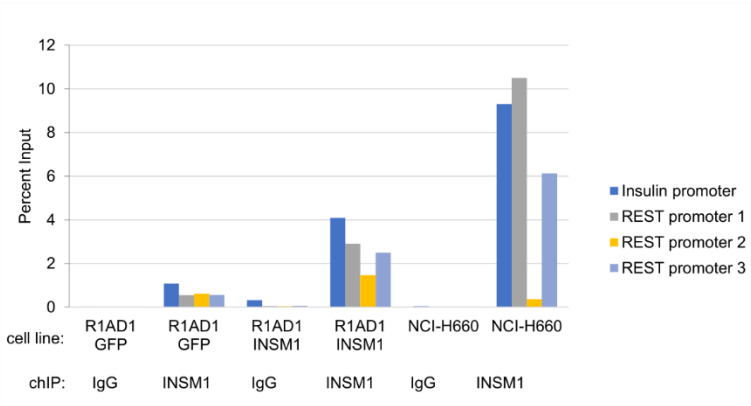

Figure 3.4 INSM1 may directly repress REST (**A**) Western Blots of REST and INSM1 in GFP or INSM1 overexpressing cell lines. (**B**) Boxplot depicting REST expression in GFP or INSM1 overexpressing models as measured by RNA-sequencing, p= Student's t-test. (**C**) Chart of predicted INSM1 motifs 1000bp upstream of the REST TSS. (**D**). Barplot depicting a representative replicate of ChIP-qpcr data for sites in the REST promoter.

A

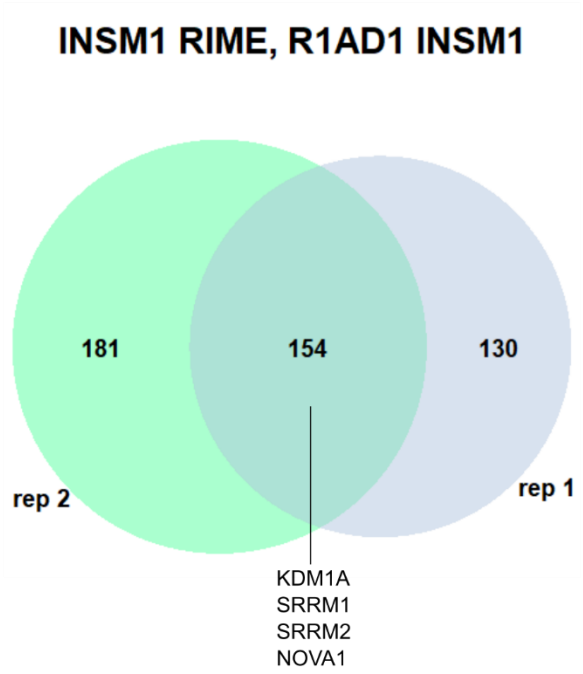

B

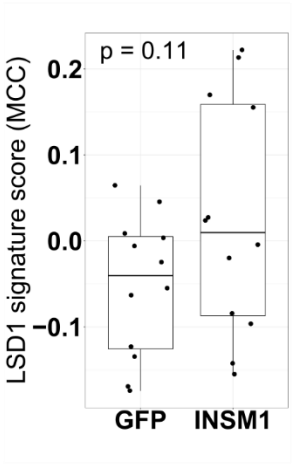

C

Sample	LSD1 signature score (MCC)
22Rv1 GFP 1	0.00398905
22Rv1 GFP 2	-0.0250966
22Rv1 INSM1 1	-0.0038705
22Rv1 INSM1 2	-0.0197886
B72 GFP 1	-0.1227312
B72 GFP 2	-0.1341368
B72 INSM1 1	-0.0838879
B72 INSM1 2	-0.0962462
LAPC4 GFP 1	-0.0053522
LAPC4 GFP 2	0.00822436
LAPC4 INSM1 1	0.02348456
LAPC4 INSM1 2	0.02693074
LNCaP AR GFP 1	-0.0553877
LNCaP AR GFP 2	-0.0624627
LNCaP AR INSM1 1	-0.1542858
LNCaP AR INSM1 2	-0.1428518
LNCaP GFP 1	-0.1686962
LNCaP GFP 2	-0.1743092
LNCaP INSM1 1	0.21331108
LNCaP INSM1 2	0.22201426
R1AD1 GFP 1	0.04610766
R1AD1 GFP 2	0.06454656
R1AD1 INSM1 1	0.15512739
R1AD1 INSM1 2	0.17000963

D

KEGG pathway	p-value
Spliceosome	1.87E-24
Ribosome biogenesis in eukaryotes	0.000144
mRNA surveillance pathway	0.000464
Mismatch repair	0.007891
Nucleotide excision repair	0.008445
RNA transport	0.025371
Base excision repair	0.033559
DNA replication	0.047121

Figure 3.5 INSM1-associated proteins detected by RIME. (**A**) Venn diagram showing overlap between replicates after IgG subtraction. (**B**) Boxplot depicting LSD1-MCC scores in engineered cell lines. (**C**) Heatmap depicting LSD1-MCC scores for individual replicates and and cell lines. (**D**) Enriched KEGG pathways in proteins associated with INSM1.

Chapter 4. Conclusions and Future Directions

The work detailed in this thesis provides insight into the features, dependencies, and potential drivers of the neuroendocrine phenotype in prostate cancer. I conducted a "pan-cancer" approach to yield insight into common developmental processes and actionable targets in a rare but increasingly more common, lethal tumor type, small cell or neuroendocrine prostate cancer (SCNPC). From this work, I identified the combination of BCL2 and WEE1 inhibition as having therapeutic efficacy in some pre-clinical models of SCNPC. I also identified a potential role for the highly expressed transcription factor, INSM1, in the development of neuroendocrine gene expression programs in prostate cancer.

Recent studies have delineated castration-resistant prostate cancer (CRPC) into five major subtypes [5]. Two of these subtypes have neuroendocrine features and are categorized by the presence of gene expression indicating an active or inactive androgen receptor (AR) pathway. In this study, I chose to focus broadly on AR-inactive neuroendocrine prostate carcinomas, termed SCNPC. Studies of another small cell or neuroendocrine tumor (SCNT), small cell lung cancer (SCLC), have revealed as many as four subtypes within SCLC delineated by the expression of the transcriptional regulators ASCL1, NEUROD1, POU2F3, and YAP1 [128]. ASCL1, NEUROD1, and POU2F3 are highly expressed in the majority of SCNPC patient samples profiled in this thesis (Figure 4), however there are a handful of samples that show selectivity for one of these genes. Similar subtyping studies are being conducted with larger panels of patient sample in SCNPC and may provide more specific insight into factors driving the development and maintenance of this phenotype.

This study provides evidence that BCL2 and WEE1 inhibition singly and/or in combination is efficacious in subsets of SCNPC (up to four of five models for the combination

tested). Mechanistic insights into the disparity of BCL2/WEE1 inhibitor phenotypes in SCNPC PDX models is hindered because the cell line models of SCNPC (NCI-H660 and MSKCC EF1) do not show a similar array of responses. Future studies involving larger cohorts or *ex vivo* culture methods of SCNPC PDX models may aid in identifying which patient population may benefit from this drug combination.

Finally, I examined a possible role for INSM1 in promoting the neuroendocrine phenotype in prostate cancer. Intriguingly, I found that INSM1 can promote neuroendocrine gene expression in some androgen-receptor dependent prostate cancer (ARPC) cell lines, but not others. My studies suggest that INSM1 may be repressing the repressor REST/NRSF, a master repressor of neural gene expression, to allow for re-expression of neuronal/neuroendocrine lineage genes. However, as INSM1 has only been described as a repressor, the full mechanism by which INSM1 can promote neuroendocrine gene expression remains an open question. What "primes" certain cell line backgrounds to be able to turn neuroendocrine gene expression programs on more easily than others? Additional studies into the gene regulatory networks active in these cell lines may begin to answer this question. Given the lack of effective therapies for SCNPC, insight into how the phenotype develops, particularly in the context of treatments that inhibit AR pathway singaling, may also yield information on how to prevent its formation.

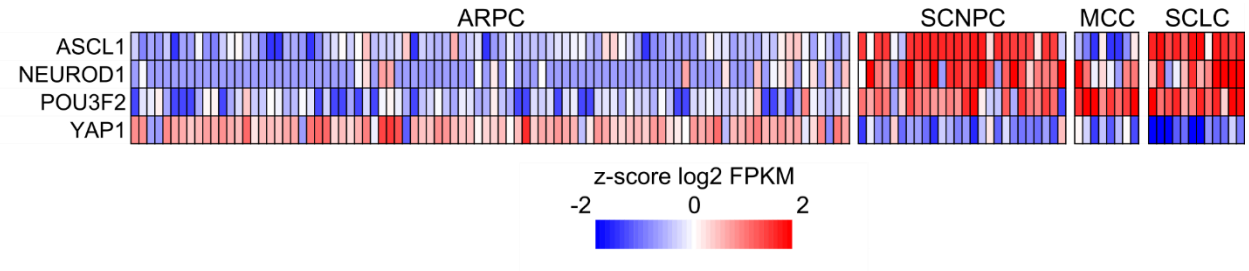

Figure 4. Heatmap depicting expression of SCLC subtype genes in RNA-sequencing panel used for this study.

References

1. Global Burden of Disease Cancer, C., et al., *Global, Regional, and National Cancer Incidence, Mortality, Years of Life Lost, Years Lived With Disability, and Disability-Adjusted Life-Years for 29 Cancer Groups, 1990 to 2017: A Systematic Analysis for the Global Burden of Disease Study.* JAMA Oncol, 2019.
2. Collin, S.M., et al., *Prostate-cancer mortality in the USA and UK in 1975-2004: an ecological study.* Lancet Oncol, 2008. **9**(5): p. 445-52.
3. Shevach, J., et al., *Concurrent Diabetes Mellitus may Negatively Influence Clinical Progression and Response to Androgen Deprivation Therapy in Patients with Advanced Prostate Cancer.* Front Oncol, 2015. **5**: p. 129.
4. Afshar, M., et al., *Shifting paradigms in the estimation of survival for castration-resistant prostate cancer: A tertiary academic center experience.* Urol Oncol, 2015. **33**(8): p. 338 e1-7.
5. Labrecque, M.P., et al., *Molecular profiling stratifies diverse phenotypes of treatment-refractory metastatic castration-resistant prostate cancer.* J Clin Invest, 2019. **130**.
6. Kumar, A., et al., *Substantial interindividual and limited intraindividual genomic diversity among tumors from men with metastatic prostate cancer.* Nat Med, 2016. **22**(4): p. 369-78.
7. Taylor, B.S., et al., *Integrative genomic profiling of human prostate cancer.* Cancer Cell, 2010. **18**(1): p. 11-22.
8. Locke, J.A., et al., *Arachidonic acid activation of intratumoral steroid synthesis during prostate cancer progression to castration resistance.* Prostate, 2010. **70**(3): p. 239-51.

9. Attard, G., C.S. Cooper, and J.S. de Bono, *Steroid hormone receptors in prostate cancer: a hard habit to break?* Cancer Cell, 2009. **16**(6): p. 458-62.

10. Bluemn, E.G., et al., *Androgen Receptor Pathway-Independent Prostate Cancer Is Sustained through FGF Signaling.* Cancer Cell, 2017. **32**(4): p. 474-489 e6.

11. Aggarwal, R., et al., *Clinical and Genomic Characterization of Treatment-Emergent Small-Cell Neuroendocrine Prostate Cancer: A Multi-institutional Prospective Study.* J Clin Oncol, 2018. **36**(24): p. 2492-2503.

12. Tetu, B., et al., *Small cell carcinoma of the prostate. Part I. A clinicopathologic study of 20 cases.* Cancer, 1987. **59**(10): p. 1803-9.

13. Epstein, J.I., et al., *Proposed morphologic classification of prostate cancer with neuroendocrine differentiation.* Am J Surg Pathol, 2014. **38**(6): p. 756-67.

14. Aparicio, A.M., et al., *Platinum-based chemotherapy for variant castrate-resistant prostate cancer.* Clin Cancer Res, 2013. **19**(13): p. 3621-30.

15. Miyoshi, Y., et al., *Neuroendocrine differentiated small cell carcinoma presenting as recurrent prostate cancer after androgen deprivation therapy.* BJU Int, 2001. **88**(9): p. 982-3.

16. Turbat-Herrera, E.A., et al., *Neuroendocrine differentiation in prostatic carcinomas. A retrospective autopsy study.* Arch Pathol Lab Med, 1988. **112**(11): p. 1100-5.

17. Shah, R.B., et al., *Androgen-independent prostate cancer is a heterogeneous group of diseases: lessons from a rapid autopsy program.* Cancer Res, 2004. **64**(24): p. 9209-16.

18. Aprikian, A.G., et al., *Neuroendocrine differentiation in metastatic prostatic adenocarcinoma.* J Urol, 1994. **151**(4): p. 914-9.

19. Tomlins, S.A., et al., *Recurrent fusion of TMPRSS2 and ETS transcription factor genes in prostate cancer.* Science, 2005. **310**(5748): p. 644-8.

20. Niederst, M.J., et al., *RB loss in resistant EGFR mutant lung adenocarcinomas that transform to small-cell lung cancer.* Nat Commun, 2015. **6**: p. 6377.

21. Oser, M.G., et al., *Transformation from non-small-cell lung cancer to small-cell lung cancer: molecular drivers and cells of origin.* Lancet Oncol, 2015. **16**(4): p. e165-72.

22. Beltran, H., et al., *Divergent clonal evolution of castration-resistant neuroendocrine prostate cancer.* Nat Med, 2016. **22**(3): p. 298-305.

23. Kim, J.Y., S.M. Hong, and J.Y. Ro, *Recent updates on grading and classification of neuroendocrine tumors.* Ann Diagn Pathol, 2017. **29**: p. 11-16.

24. Meis-Kindblom, J.M., G. Stenman, and L.G. Kindblom, *Differential diagnosis of small round cell tumors.* Semin Diagn Pathol, 1996. **13**(3): p. 213-41.

25. Brodeur, G.M., et al., *Amplification of N-myc in untreated human neuroblastomas correlates with advanced disease stage.* Science, 1984. **224**(4653): p. 1121-4.

26. Seeger, R.C., et al., *Association of multiple copies of the N-myc oncogene with rapid progression of neuroblastomas.* N Engl J Med, 1985. **313**(18): p. 1111-6.

27. George, J., et al., *Comprehensive genomic profiles of small cell lung cancer.* Nature, 2015. **524**(7563): p. 47-53.

28. Peifer, M., et al., *Integrative genome analyses identify key somatic driver mutations of small-cell lung cancer.* Nat Genet, 2012. **44**(10): p. 1104-10.

29. Beltran, H., et al., *Molecular characterization of neuroendocrine prostate cancer and identification of new drug targets.* Cancer Discov, 2011. **1**(6): p. 487-95.

30. Nguyen, H.M., et al., *LuCaP Prostate Cancer Patient-Derived Xenografts Reflect the Molecular Heterogeneity of Advanced Disease an--d Serve as Models for Evaluating Cancer Therapeutics.* Prostate, 2017. **77**(6): p. 654-671.

31. Carney, D.N., et al., *Establishment and identification of small cell lung cancer cell lines having classic and variant features.* Cancer Res, 1985. **45**(6): p. 2913-23.

32. Mertz, K.D., et al., *Molecular characterization of TMPRSS2-ERG gene fusion in the NCI-H660 prostate cancer cell line: a new perspective for an old model.* Neoplasia, 2007. **9**(3): p. 200-6.

33. Paulson, K.G., et al., *Transcriptome-wide studies of merkel cell carcinoma and validation of intratumoral CD8+ lymphocyte invasion as an independent predictor of survival.* J Clin Oncol, 2011. **29**(12): p. 1539-46.

34. Bobos, M., et al., *Immunohistochemical distinction between merkel cell carcinoma and small cell carcinoma of the lung.* Am J Dermatopathol, 2006. **28**(2): p. 99-104.

35. Leech, S.N., et al., *Merkel cell carcinoma can be distinguished from metastatic small cell carcinoma using antibodies to cytokeratin 20 and thyroid transcription factor 1.* J Clin Pathol, 2001. **54**(9): p. 727-9.

36. Teratani-Ota, Y., et al., *Induction of specific neuron types by overexpression of single transcription factors.* In Vitro Cell Dev Biol Anim, 2016. **52**(9): p. 961-973.

37. Henry, C., A.F. Close, and J. Buteau, *A critical role for the neural zinc factor ST18 in pancreatic beta-cell apoptosis.* J Biol Chem, 2014. **289**(12): p. 8413-9.

38. Mall, M., et al., *Myt1l safeguards neuronal identity by actively repressing many non-neuronal fates.* Nature, 2017. **544**(7649): p. 245-249.

39. Vierbuchen, T., et al., *Direct conversion of fibroblasts to functional neurons by defined factors.* Nature, 2010. **463**(7284): p. 1035-41.

40. Lastowska, M., et al., *Identification of a neuronal transcription factor network involved in medulloblastoma development.* Acta Neuropathol Commun, 2013. **1**: p. 35.

41. Fleming, W.H., et al., *Expression of the c-myc protooncogene in human prostatic carcinoma and benign prostatic hyperplasia.* Cancer Res, 1986. **46**(3): p. 1535-8.

42. Buttyan, R., et al., *Enhanced expression of the c-myc protooncogene in high-grade human prostate cancers.* Prostate, 1987. **11**(4): p. 327-37.

43. Hawksworth, D., et al., *Overexpression of C-MYC oncogene in prostate cancer predicts biochemical recurrence.* Prostate Cancer Prostatic Dis, 2010. **13**(4): p. 311-5.

44. Kim, D.W., et al., *Genetic requirement for Mycl and efficacy of RNA Pol I inhibition in mouse models of small cell lung cancer.* Genes Dev, 2016. **30**(11): p. 1289-99.

45. Ward, M., et al., *Conservation and tissue-specific transcription patterns of long noncoding RNAs.* J Hum Transcr, 2015. **1**(1): p. 2-9.

46. Brunner, A.L., et al., *Transcriptional profiling of long non-coding RNAs and novel transcribed regions across a diverse panel of archived human cancers.* Genome Biol, 2012. **13**(8): p. R75.

47. Bhan, A., M. Soleimani, and S.S. Mandal, *Long Noncoding RNA and Cancer: A New Paradigm.* Cancer Res, 2017. **77**(15): p. 3965-3981.

48. Prensner, J.R., et al., *The long noncoding RNA SChLAP1 promotes aggressive prostate cancer and antagonizes the SWI/SNF complex.* Nat Genet, 2013. **45**(11): p. 1392-8.

49. Zhang, A., et al., *LncRNA HOTAIR Enhances the Androgen-Receptor-Mediated Transcriptional Program and Drives Castration-Resistant Prostate Cancer.* Cell Rep, 2015. **13**(1): p. 209-221.

50. Ramnarine, V.R., et al., *The long noncoding RNA landscape of neuroendocrine prostate cancer and its clinical implications.* Gigascience, 2018. **7**(6).

51. Finan, C., et al., *The druggable genome and support for target identification and validation in drug development.* Sci Transl Med, 2017. **9**(383).

52. Rudin, C.M., et al., *Rovalpituzumab tesirine, a DLL3-targeted antibody-drug conjugate, in recurrent small-cell lung cancer: a first-in-human, first-in-class, open-label, phase 1 study.* Lancet Oncol, 2017. **18**(1): p. 42-51.

53. Lenhart, R., et al., *Sensitivity of Small Cell Lung Cancer to BET Inhibition Is Mediated by Regulation of ASCL1 Gene Expression.* Mol Cancer Ther, 2015. **14**(10): p. 2167-74.

54. Puissant, A., et al., *Targeting MYCN in neuroblastoma by BET bromodomain inhibition.* Cancer Discov, 2013. **3**(3): p. 308-23.

55. Kato, F., et al., *MYCL is a target of a BET bromodomain inhibitor, JQ1, on growth suppression efficacy in small cell lung cancer cells.* Oncotarget, 2016. **7**(47): p. 77378-77388.

56. Faivre, E.J., et al., *Selective inhibition of the BD2 bromodomain of BET proteins in prostate cancer.* Nature, 2020. **578**(7794): p. 306-310.

57. Lochmann, T.L., et al., *Venetoclax Is Effective in Small-Cell Lung Cancers with High BCL-2 Expression.* Clin Cancer Res, 2018. **24**(2): p. 360-369.

58. Verhaegen, M.E., et al., *Merkel cell carcinoma dependence on bcl-2 family members for survival.* J Invest Dermatol, 2014. **134**(8): p. 2241-2250.

59. Sanchez-Vega, F., et al., *Oncogenic Signaling Pathways in The Cancer Genome Atlas.* Cell, 2018. **173**(2): p. 321-337 e10.

60. Hoadley, K.A., et al., *Cell-of-Origin Patterns Dominate the Molecular Classification of 10,000 Tumors from 33 Types of Cancer.* Cell, 2018. **173**(2): p. 291-304 e6.

61. Dasari, A., et al., *Trends in the Incidence, Prevalence, and Survival Outcomes in Patients With Neuroendocrine Tumors in the United States.* JAMA Oncol, 2017. **3**(10): p. 1335-1342.

62. Mosquera, J.M., et al., *Concurrent AURKA and MYCN gene amplifications are harbingers of lethal treatment-related neuroendocrine prostate cancer.* Neoplasia, 2013. **15**(1): p. 1-10.

63. Rickman, D.S., J.H. Schulte, and M. Eilers, *The Expanding World of N-MYC-Driven Tumors.* Cancer Discov, 2018. **8**(2): p. 150-163.

64. Zhang, Y. and L. Tang, *The Application of lncRNAs in Cancer Treatment and Diagnosis.* Recent Pat Anticancer Drug Discov, 2018. **13**(3): p. 292-301.

65. Crea, F., et al., *The role of epigenetics and long noncoding RNA MIAT in neuroendocrine prostate cancer.* Epigenomics, 2016. **8**(5): p. 721-31.

66. Beltran, H., et al., *A Phase II Trial of the Aurora Kinase A Inhibitor Alisertib for Patients with Castration-resistant and Neuroendocrine Prostate Cancer: Efficacy and Biomarkers.* Clin Cancer Res, 2019. **25**(1): p. 43-51.

67. Segal, N.H., et al., *BCL-2 proto-oncogene expression in prostate cancer and its relationship to the prostatic neuroendocrine cell.* Arch Pathol Lab Med, 1994. **118**(6): p. 616-8.

68. Brambilla, E., et al., *Apoptosis-related factors p53, Bcl2, and Bax in neuroendocrine lung tumors.* Am J Pathol, 1996. **149**(6): p. 1941-52.

69. Mohler, J.L., et al., *Prostate Cancer, Version 2.2019, NCCN Clinical Practice Guidelines in Oncology.* J Natl Compr Canc Netw, 2019. **17**(5): p. 479-505.

70. Lee, J.K., et al., *N-Myc Drives Neuroendocrine Prostate Cancer Initiated from Human Prostate Epithelial Cells.* Cancer Cell, 2016. **29**(4): p. 536-547.

71. Rudin, C.M., et al., *Comprehensive genomic analysis identifies SOX2 as a frequently amplified gene in small-cell lung cancer.* Nat Genet, 2012. **44**(10): p. 1111-6.

72. Huang, M. and W.A. Weiss, *Neuroblastoma and MYCN.* Cold Spring Harb Perspect Med, 2013. **3**(10): p. a014415.

73. Lewin, J., et al., *Phase Ib Trial With Birabresib, a Small-Molecule Inhibitor of Bromodomain and Extraterminal Proteins, in Patients With Selected Advanced Solid Tumors.* J Clin Oncol, 2018. **36**(30): p. 3007-3014.

74. Roudier, M.P., et al., *Characterizing the molecular features of ERG-positive tumors in primary and castration resistant prostate cancer.* Prostate, 2016. **76**(9): p. 810-22.

75. Butterworth, M., et al., *BH3 profiling and a toolkit of BH3-mimetic drugs predict anti-apoptotic dependence of cancer cells.* Br J Cancer, 2016. **114**(6): p. 638-41.

76. Shamas-Din, A., et al., *Mechanisms of action of Bcl-2 family proteins.* Cold Spring Harb Perspect Biol, 2013. **5**(4): p. a008714.

77. Greco, W.R., G. Bravo, and J.C. Parsons, *The search for synergy: a critical review from a response surface perspective.* Pharmacol Rev, 1995. **47**(2): p. 331-85.

78. Chou, T.C., *Theoretical basis, experimental design, and computerized simulation of synergism and antagonism in drug combination studies.* Pharmacol Rev, 2006. **58**(3): p. 621-81.

79. Sakurikar, N., J.M. Eichhorn, and T.C. Chambers, *Cyclin-dependent kinase-1 (Cdk1)/cyclin B1 dictates cell fate after mitotic arrest via phosphoregulation of antiapoptotic Bcl-2 proteins.* J Biol Chem, 2012. **287**(46): p. 39193-204.

80. Zhou, L., et al., *CDK1 switches mitotic arrest to apoptosis by phosphorylating Bcl-2/Bax family proteins during treatment with microtubule interfering agents.* Cell Biol Int, 2014. **38**(6): p. 737-46.

81. Castle, V.P., et al., *Expression of the apoptosis-suppressing protein bcl-2, in neuroblastoma is associated with unfavorable histology and N-myc amplification.* Am J Pathol, 1993. **143**(6): p. 1543-50.

82. Vaux, D.L., S. Cory, and J.M. Adams, *Bcl-2 gene promotes haemopoietic cell survival and cooperates with c-myc to immortalize pre-B cells.* Nature, 1988. **335**(6189): p. 440-2.

83. Ott, G., A. Rosenwald, and E. Campo, *Understanding MYC-driven aggressive B-cell lymphomas: pathogenesis and classification.* Blood, 2013. **122**(24): p. 3884-91.

84. Augustyn, A., et al., *ASCL1 is a lineage oncogene providing therapeutic targets for high-grade neuroendocrine lung cancers.* Proc Natl Acad Sci U S A, 2014. **111**(41): p. 14788-93.

85. Rapa, I., et al., *Human ASH1 expression in prostate cancer with neuroendocrine differentiation.* Mod Pathol, 2008. **21**(6): p. 700-7.

86. Chteinberg, E., et al., *Neuroendocrine Key Regulator Gene Expression in Merkel Cell Carcinoma.* Neoplasia, 2018. **20**(12): p. 1227-1235.

87. R, S.S. and A. Eastman, *BCL2 Inhibitors as Anticancer Drugs: A Plethora of Misleading BH3 Mimetics.* Mol Cancer Ther, 2016. **15**(9): p. 2011-7.

88. Pei, S., et al., *Monocytic Subclones Confer Resistance to Venetoclax-Based Therapy in Patients with Acute Myeloid Leukemia.* Cancer Discov, 2020. **10**(4): p. 536-551.

89. Inuzuka, H., et al., *SCF(FBW7) regulates cellular apoptosis by targeting MCL1 for ubiquitylation and destruction.* Nature, 2011. **471**(7336): p. 104-9.

90. Wertz, I.E., et al., *Sensitivity to antitubulin chemotherapeutics is regulated by MCL1 and FBW7.* Nature, 2011. **471**(7336): p. 110-4.

91. Terrano, D.T., M. Upreti, and T.C. Chambers, *Cyclin-dependent kinase 1-mediated Bcl-xL/Bcl-2 phosphorylation acts as a functional link coupling mitotic arrest and apoptosis.* Mol Cell Biol, 2010. **30**(3): p. 640-56.

92. Lapuk, A.V., et al., *From sequence to molecular pathology, and a mechanism driving the neuroendocrine phenotype in prostate cancer.* J Pathol, 2012. **227**(3): p. 286-97.

93. Pinnoji, R.C., et al., *Repressor element-1 silencing transcription factor/neuronal restrictive silencer factor (REST/NRSF) can regulate HSV-1 immediate-early transcription via histone modification.* Virol J, 2007. **4**: p. 56.

94. Ooi, L. and I.C. Wood, *Chromatin crosstalk in development and disease: lessons from REST.* Nat Rev Genet, 2007. **8**(7): p. 544-54.

95. Ballas, N. and G. Mandel, *The many faces of REST oversee epigenetic programming of neuronal genes.* Curr Opin Neurobiol, 2005. **15**(5): p. 500-6.

96. Palm, K., et al., *Neuronal expression of zinc finger transcription factor REST/NRSF/XBR gene.* J Neurosci, 1998. **18**(4): p. 1280-96.

97. Raj, B., et al., *Cross-regulation between an alternative splicing activator and a transcription repressor controls neurogenesis.* Mol Cell, 2011. **43**(5): p. 843-50.

98. Zhang, X., et al., *SRRM4 Expression and the Loss of REST Activity May Promote the Emergence of the Neuroendocrine Phenotype in Castration-Resistant Prostate Cancer.* Clin Cancer Res, 2015. **21**(20): p. 4698-708.

99. Li, Y., et al., *SRRM4 Drives Neuroendocrine Transdifferentiation of Prostate Adenocarcinoma Under Androgen Receptor Pathway Inhibition.* Eur Urol, 2017. **71**(1): p. 68-78.

100. Goto, Y., et al., *A novel human insulinoma-associated cDNA, IA-1, encodes a protein with "zinc-finger" DNA-binding motifs.* J Biol Chem, 1992. **267**(21): p. 15252-7.

101. Lan, M.S. and M.B. Breslin, *Structure, expression, and biological function of INSM1 transcription factor in neuroendocrine differentiation.* FASEB J, 2009. **23**(7): p. 2024-33.

102. Farkas, L.M., et al., *Insulinoma-associated 1 has a panneurogenic role and promotes the generation and expansion of basal progenitors in the developing mouse neocortex.* Neuron, 2008. **60**(1): p. 40-55.

103. Osipovich, A.B., et al., *Insm1 promotes endocrine cell differentiation by modulating the expression of a network of genes that includes Neurog3 and Ripply3.* Development, 2014. **141**(15): p. 2939-49.

104. Breslin, M.B., M. Zhu, and M.S. Lan, *NeuroD1/E47 regulates the E-box element of a novel zinc finger transcription factor, IA-1, in developing nervous system.* J Biol Chem, 2003. **278**(40): p. 38991-7.

105. Lan, M.S., et al., *IA-1, a new marker for neuroendocrine differentiation in human lung cancer cell lines.* Cancer Res, 1993. **53**(18): p. 4169-71.

106. Lilo, M.T., Y. Chen, and R.E. LeBlanc, *INSM1 Is More Sensitive and Interpretable than Conventional Immunohistochemical Stains Used to Diagnose Merkel Cell Carcinoma.* Am J Surg Pathol, 2018. **42**(11): p. 1541-1548.

107. Monaghan, C.E., et al., *REST corepressors RCOR1 and RCOR2 and the repressor INSM1 regulate the proliferation-differentiation balance in the developing brain.* Proc Natl Acad Sci U S A, 2017. **114**(3): p. E406-E415.

108. Fujino, K., et al., *Insulinoma-Associated Protein 1 Is a Crucial Regulator of Neuroendocrine Differentiation in Lung Cancer.* Am J Pathol, 2015. **185**(12): p. 3164-77.

109. Mohammed, H., et al., *Endogenous purification reveals GREB1 as a key estrogen receptor regulatory factor.* Cell Rep, 2013. **3**(2): p. 342-9.

110. Chen, C., M.B. Breslin, and M.S. Lan, *Sonic hedgehog signaling pathway promotes INSM1 transcription factor in neuroendocrine lung cancer.* Cell Signal, 2018. **46**: p. 83-91.

111. Nyquist, M.D., et al., *Molecular determinants of response to high-dose androgen therapy in prostate cancer.* JCI Insight, 2019. **4**(19).

112. Labrecque, M.P., et al., *Molecular profiling stratifies diverse phenotypes of treatment-refractory metastatic castration-resistant prostate cancer.* J Clin Invest, 2019. **130**: p. 4492-4505.

113. Ostano, P., et al., *Gene Expression Signature Predictive of Neuroendocrine Transformation in Prostate Adenocarcinoma.* Int J Mol Sci, 2020. **21**(3).

114. Rodriguez-Zarco, E., et al., *Immunohistochemical study of the neural development transcription factors (TTF1, ASCL1 and BRN2) in neuroendocrine prostate tumours.* Actas Urol Esp, 2017. **41**(8): p. 529-534.

115. Liu, W.D., et al., *INSM1 functions as a transcriptional repressor of the neuroD/beta2 gene through the recruitment of cyclin D1 and histone deacetylases.* Biochem J, 2006. **397**(1): p. 169-77.

116. Fornes, O., et al., *JASPAR 2020: update of the open-access database of transcription factor binding profiles.* Nucleic Acids Res, 2020. **48**(D1): p. D87-D92.

117. Wang, H.W., et al., *Identification of an INSM1-binding site in the insulin promoter: negative regulation of the insulin gene transcription.* J Endocrinol, 2008. **198**(1): p. 29-39.

118. Takagi, S., et al., *LSD1 Inhibitor T-3775440 Inhibits SCLC Cell Proliferation by Disrupting LSD1 Interactions with SNAG Domain Proteins INSM1 and GFI1B.* Cancer Res, 2017. **77**(17): p. 4652-4662.

119. Park, D.E., et al., *Merkel cell polyomavirus activates LSD1-mediated blockade of non-canonical BAF to regulate transformation and tumorigenesis.* Nat Cell Biol, 2020.

120. Borges, M., et al., *An achaete-scute homologue essential for neuroendocrine differentiation in the lung.* Nature, 1997. **386**(6627): p. 852-5.

121. Jiang, T., et al., *Achaete-scute complex homologue 1 regulates tumor-initiating capacity in human small cell lung cancer.* Cancer Res, 2009. **69**(3): p. 845-54.

122. Ketscher, A., et al., *LSD1 controls metastasis of androgen-independent prostate cancer cells through PXN and LPAR6.* Oncogenesis, 2014. **3**: p. e120.

123. Liang, Y., et al., *LSD1-Mediated Epigenetic Reprogramming Drives CENPE Expression and Prostate Cancer Progression.* Cancer Res, 2017. **77**(20): p. 5479-5490.

124. Kashyap, V., et al., *The lysine specific demethylase-1 (LSD1/KDM1A) regulates VEGF-A expression in prostate cancer.* Mol Oncol, 2013. **7**(3): p. 555-66.

125. Sehrawat, A., et al., *LSD1 activates a lethal prostate cancer gene network independently of its demethylase function.* Proc Natl Acad Sci U S A, 2018. **115**(18): p. E4179-E4188.

126. Mohammad, H.P., et al., *A DNA Hypomethylation Signature Predicts Antitumor Activity of LSD1 Inhibitors in SCLC.* Cancer Cell, 2015. **28**(1): p. 57-69.

127. Lee, C., et al., *Lsd1 as a therapeutic target in Gfi1-activated medulloblastoma.* Nat Commun, 2019. **10**(1): p. 332.

128. Rudin, C.M., et al., *Molecular subtypes of small cell lung cancer: a synthesis of human and mouse model data.* Nat Rev Cancer, 2019. **19**(5): p. 289-297.